Localized charge carriers in graphene nanodevices

D. Bischoff, A. Varlet, P. Simonet, M. Eich, H. C. Overweg, T. Ihn, and K. Ensslin

Citation: Applied Physics Reviews **2**, 031301 (2015); doi: 10.1063/1.4926448
View online: http://dx.doi.org/10.1063/1.4926448
View Table of Contents: http://scitation.aip.org/content/aip/journal/apr2/2/3?ver=pdfcov
Published by the AIP Publishing

APPLIED PHYSICS REVIEWS

Localized charge carriers in graphene nanodevices

D. Bischoff,[a)] A. Varlet, P. Simonet, M. Eich, H. C. Overweg, T. Ihn, and K. Ensslin
Solid State Physics Laboratory, ETH Zurich, 8093 Zurich, Switzerland

(Received 2 March 2015; accepted 4 June 2015; published online 17 July 2015)

Graphene—two-dimensional carbon—is a material with unique mechanical, optical, chemical, and electronic properties. Its use in a wide range of applications was therefore suggested. From an electronic point of view, nanostructured graphene is of great interest due to the potential opening of a band gap, applications in quantum devices, and investigations of physical phenomena. Narrow graphene stripes called "nanoribbons" show clearly different electronical transport properties than micron-sized graphene devices. The conductivity is generally reduced and around the charge neutrality point, the conductance is nearly completely suppressed. While various mechanisms can lead to this observed suppression of conductance, disordered edges resulting in localized charge carriers are likely the main cause in a large number of experiments. Localized charge carriers manifest themselves in transport experiments by the appearance of Coulomb blockade diamonds. This review focuses on the mechanisms responsible for this charge localization, on interpreting the transport details, and on discussing the consequences for physics and applications. Effects such as multiple coupled sites of localized charge, cotunneling processes, and excited states are discussed. Also, different geometries of quantum devices are compared. Finally, an outlook is provided, where open questions are addressed. © *2015 AIP Publishing LLC*. [http://dx.doi.org/10.1063/1.4926448]

TABLE OF CONTENTS

[a)]Electronic mail: dominikb@phys.ethz.ch

I. INTRODUCTION

A. Two-dimensional carbon

Graphene—currently the thinnest existing material—consists of a single layer of carbon atoms. Each carbon atom is covalently bonded to its three nearest neighbors, thereby forming a honeycomb crystal structure. Graphene can therefore be considered as a truly two-dimensional crystal. The name "graphene" originates from graphite, which itself consists of a thick stack of individual graphene layers, bonded to each other by van-der-Waals forces. Graphene is also closely related to carbon nanotubes, which can be thought of as rolled-up graphene sheets, as well as diamond, which is covalently bonded carbon in three dimensions.

As graphene is part of this family of famous and technologically relevant carbon materials, it is rather surprising that the first experiments date back to only 2004.[1] While thin layers of covalently (sp^2) bonded carbon were produced much earlier,[2,3] the fast expansion of the research field after the experiment in 2004 can be attributed to the ease with which high quality graphene was obtained and characterized.

Graphene is also a material of many superlatives. Owing to the covalent carbon-carbon bond, it is among the strongest and most stretchable materials investigated so far.[4,5] It is chemically quite inert and has, at the same time, a huge surface to volume ratio which makes it sensitive enough to detect single adsorbed molecules.[6] Furthermore, graphene is optically nearly transparent,[7] is one of the best conductors of heat,[8] and supports the highest ever measured current densities at room temperature.[9]

B. Electrons in graphene are special

As graphene is the basic building block for graphite, which itself is the key component of various applications including nuclear reactors, it was theoretically heavily studied since the late 1940s.[10] The crystal lattice is built from a basis of two carbon atoms that are arranged in space to form a hexagonal lattice. The band structure also possesses this two-fold degeneracy manifesting itself in the K and K' points in the Brillouin zone where bands cross each other. For undoped graphene, the Fermi energy is located at the crossing points of the bands. Graphene is therefore a semimetal or zero band gap semiconductor. In a perfect crystal, the bands at K and K' are indistinguishable and are often described with the term "valley degeneracy." In contrast to most of the other materials used in electronics which exhibit parabolic electronic bands, graphene exhibits a linear E(k) relation at low energies as schematically depicted in Fig. 1. Most of the properties of graphene originate from this special crystal and band structure. As there are a number of excellent theoretical reviews[11–13] about graphene, only a few key concepts important for graphene nanodevices will be discussed here.

Due to the special band structure, electrons and holes in graphene exhibit in theory the same properties with exception of having the opposite charge. Also, as a result of the band structure, a phenomenon called "Klein tunneling"[14,15] occurs in graphene: electrons (and holes) have a low backscattering probability when crossing from an n-doped to a p-doped region. This is in stark contrast to most other materials and results in long electronic mean free paths even at elevated temperatures.[16]

Owing to its special electronic properties, graphene was suggested for multiple electronic applications. However, not all of the superlatives are intrinsically favorable for electronic devices. Because of the large surface, graphene is extremely sensitive to its environment. In order to fabricate devices with high quality, contaminations and the substrate need to be considered carefully.

Another issue for electronics is that most of the designs for modern electronics require a semiconductor with a sufficiently large band gap. Many of graphene's special electronic properties, however, rely on the linear band structure having no band gap. For traditional field effect transistor designs, for example, this results in very low on-off ratios and renders the devices not useful for digital applications.[17] The problem is less severe for high frequency transistors.[18] One way to circumvent the problem of the zero band gap is to alter graphene such that a band gap opens. This can be achieved by chemical functionalization with, for example, hydrogen[19] or fluorine.[20] Alternatively, a band gap can be opened by applying a perpendicular electric field to bilayer

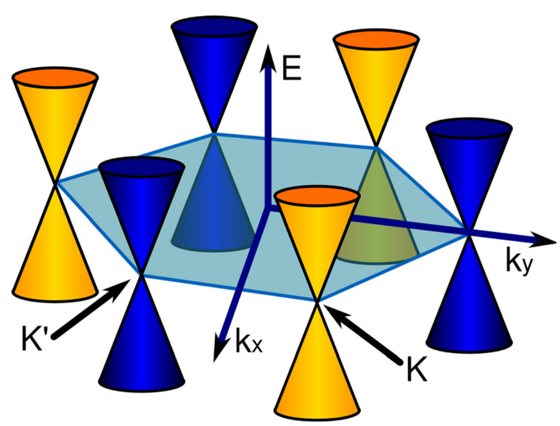

FIG. 1. Schematic of the low energy part of the graphene band structure. Marked in light blue is the Brillouin zone, Dirac cones at K are colored yellow, and Dirac cones at K' are colored blue.

graphene.[21] A more promising route is however to use novel device designs that benefit from the properties of graphene rather than trying to correct them. Examples for such devices are tunneling transistors.[22,23]

C. Graphene nanostructure quantum devices

Another route for changing graphene such that it obtains a band gap is to cut it into narrow stripes[24] called "nanoribbons" or "nanoconstrictions." Such a device is shown in Fig. 2. This approach of fabricating narrow devices is further interesting as digital electronics generally profit from smaller device sizes.

Graphene nanostructures are also intriguing from a quantum physics point of view: graphene quantum dots (see Fig. 3) were early on suggested as ideal devices for quantum computing as long spin coherence times are expected.[25–27] The principle reasoning is simple: spin-orbit interactions[28] as well as hyperfine interactions (nearly 99% of all carbon atoms are of the C-12 isotope type and have no nuclear spin) are expected to be low. These two effects were found to strongly limit spin lifetimes in GaAs quantum dots.[29,30] There are some indications that imperfections in graphene might lead to a significantly lower spin lifetime,[31] but this problem can, in principle, be solved by fabricating devices of better quality.

Other suggested and experimentally realized quantum devices are ring shaped structures used to investigate electron interference.[32–37] There are many theoretical proposals for quantum devices such as, for example, spin valves[38] or quantum spin Hall devices.[39] The experimental realization of most of these suggested devices is, however, not yet possible as they rely on special structures with atomic precision.

When comparing the conductivity of micron sized graphene devices with nanoribbons, two striking differences are typically observed: the conductivity of the wide device is significantly higher and a region in gate voltage (carrier density) of strongly suppressed conductivity is visible in the nanoribbon device close to the charge neutrality point. Such a comparison is shown in Fig. 4. Two effects might start to play a role for narrow devices: quantum confinement ("particle in a box") and edges. Along similar lines, the question appears at which dimensions the bulk graphene properties (linear band structure, Klein tunneling, linear density of states in energy, etc.) disappear in nanostructures.

Many open questions also exist for graphene quantum dots. For quantum dots in other material systems, a number of phenomena were observed such as spin blockade,[29] Kondo effect in quantum dots,[41,42] shell filling,[43] and

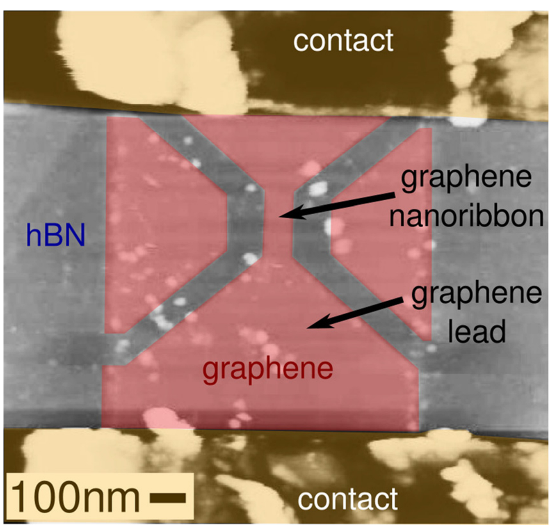

FIG. 2. Scanning force microscopy (SFM) image of a single layer graphene nanoribbon (highlighted in red) on a hexagonal boron nitride (hBN) substrate with gold contacts on top and bottom. For the rest of this review, the term "nanoribbon" will be used for graphene stripes that have a width of the order of 100 nm or smaller. The width is generally constant and might increase towards the lead regions.

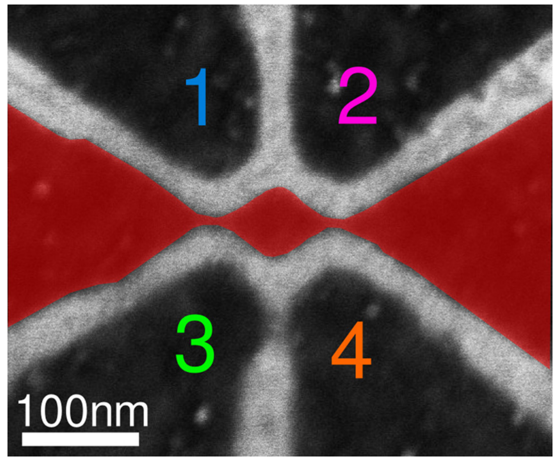

FIG. 3. Scanning electron microscopy (SEM) image of a bilayer graphene quantum dot (highlighted in red) with side gates 1–4 (device from Ref. 40). A quantum dot is a device consisting of a small conductive island onto which single charges can be loaded. The island is generally weakly coupled to its environment. The combination of Coulomb energy and quantum confinement terms leads to a discrete energy spectrum. This discrete energy spectrum can be probed experimentally and Coulomb blockade can be observed. A double quantum dot consists of two such islands coupled to each other. Single electron transistors (SETs) which are larger quantum dots where only the Coulomb energy is relevant will also be called quantum dots for the rest of this review in order to simplify the notation.

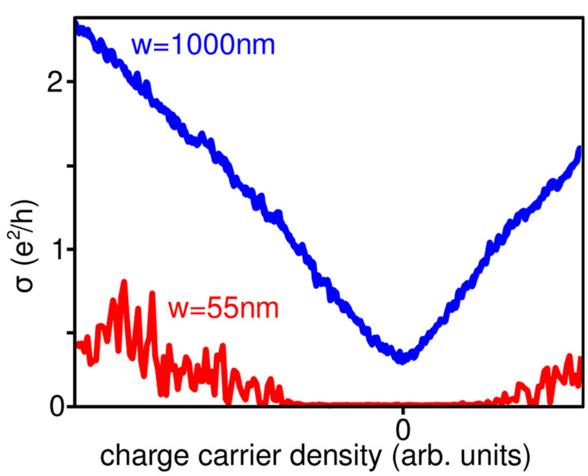

FIG. 4. Conductivity of a wide (blue) and a narrow (red) graphene stripe at a temperature of 4.2 K. The *x*-axis of both curves is not identical but comparable.

electronic excited states.[44] While features resembling electronic excited states were reported for various measurements in graphene quantum dots, unresolved questions exist.[45] Spin blockade was so far not observed at all in graphene quantum dot systems, and the Kondo effect as well as shell filling were reported for only one device.[46]

D. Scope of this review

This review provides a general overview of the current state of the art in the field of graphene nanodevices. Special focus is put on electronic transport experiments at cryogenic temperatures as the experimental energy resolution at low temperatures is increased. Since graphene nanoribbons (nanoconstrictions) are the basic building block for any graphene nanodevice, they are discussed in depth. The main part of this review focuses on the physical processes leading to charge localization in graphene nanodevices and their consequences for electronic transport. Consequently, aspects such as disorder from the environment and edges need to be discussed, as well as theoretical approaches for modeling those effects. Finally, graphene quantum dots are briefly discussed, again focusing on the physics governing transport through those structures. Here, the focus is put on experiments that were not already discussed in the review in Ref. 47.

E. Organization of this review

This review is organized as follows. Section II gives a short introduction about substrate and contamination related issues for micron sized graphene devices. Substrate, contamination, and defects define the general material quality and will ultimately also have an influence on the properties of nanodevices. Section III introduces graphene edges starting with perfect edges and reconstructed edges following principal crystal directions. Graphene edges have a direct impact on the bandstructure of graphene nanoribbons and therefore on their electronic properties. Section IV provides a short overview of how graphene nanostructures with disordered edges can be treated in numerical simulations. The role played by disordered edges is important in experiment as it is so far challenging to fabricate devices with perfect edges. Section V discusses experiments where different pristine and disordered graphene edges were imaged. Sections VI and VII provide an extensive overview of the different fabrication processes that can be used to pattern graphene nanostructures for electronical transport experiments. Different fabrication processes will result in different edge morphologies, defects, and disorder which might in turn strongly influence the electronic transport properties. Section VIII discusses electronic transport experiments in graphene nanoribbons in detail. Charge localization, transport mechanisms, and alternative explanations are discussed in detail. Section IX extends the discussion to island-shaped graphene nanodevices with a focus on general transport properties rather than a focus on special effects. This section is to be seen as an extension of Sec. VIII for devices that have a different geometry. In Sec. X, the findings of this review paper are summarized and put into perspective. Section XI highlights unresolved questions and provides ideas for future experiments. Appendix A clarifies how the authors use the term "band gap." Appendix B lists a number of abbreviations used in this review.

II. SUBSTRATES AND ENVIRONMENT

For large scale graphene devices, it has been shown that the substrate as well as the cleanliness of the devices have a strong influence on transport properties. These effects might therefore also play an important role for graphene nanodevices and are briefly discussed in this section.

Typical micron sized graphene devices on a silicon dioxide (SiO_2) substrate exhibit charge carrier mobilities of around 10 000 $cm^2V^{-1}s^{-1}$ or lower and disorder densities of around 10^{11} cm^{-2} or higher.[48,49] The disorder density is a measure for the disorder potential originating from impurities and the substrate.[50] A shift of the charge neutrality point to high back-gate voltage is not uncommon and indicates high overall doping levels.[1]

A first significant improvement of the transport properties of graphene devices was achieved when they were suspended[51] and current annealed:[52] low temperature mobilities exceeding 100 000 $cm^2V^{-1}s^{-1}$ and disorder densities lower than 10^{10} cm^{-2} were obtained.[49,53,54] Further improvements in fabrication and annealing[55] allowed for mobilities exceeding 10^6 $cm^2V^{-1}s^{-1}$ and disorder densities as low as 10^8 cm^{-2}.

Suspended graphene devices have, however, several inherent limitations: their length is limited to micrometers,[56] and the maximal applicable back-gate voltage (and thereby the maximum charge carrier density) is small due to bending of the graphene.[57] It is furthermore challenging to fabricate multi-terminal devices,[58,59] top gates,[59–61] and nanostructures.[56,62]

Another breakthrough was achieved with the fabrication of graphene devices on hexagonal boron nitride (hBN) as shown in Fig. 5.[63] First graphene devices on hBN were comparable to suspended devices in terms of mobility and disorder density.[63] There are a number of factors that might be

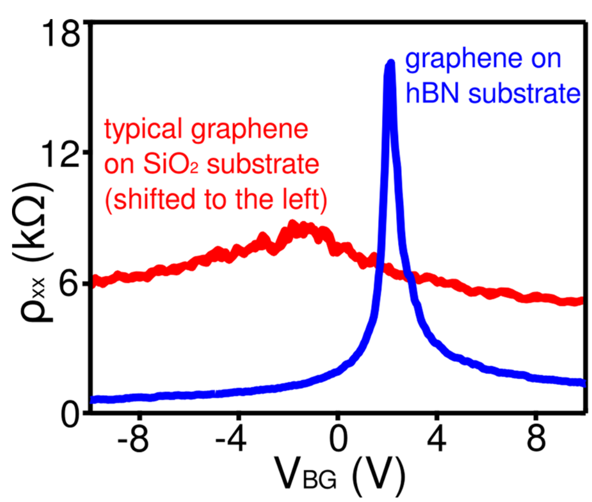

FIG. 5. Comparison of the resistivity as a function of applied back-gate voltage for a micron sized graphene device on SiO_2 (red) and on hBN (blue).

responsible for the enhanced performance compared to devices on silicon dioxide: a flatter substrate,[63] less charged impurities in the substrate,[64] and successful thermal annealing[65] leading to less disorder.[66,67]

The next significant improvement in the quality of graphene devices was achieved when they were encapsulated with an additional layer of hBN.[16] Atomically clean interfaces can be obtained with this method and the graphene is protected from further contaminations.[68]

The latest improvement in technology and cleanliness was obtained by the development of a process in which the graphene flake never comes in contact with photo- or electron beam lithography (EBL) resist: graphene and hBN are stacked on top of each other with a "pick-up" process and contacts are fabricated at the side by etching through the complete stack.[69–72] An issue that is so far not fully resolved is that hydrocarbons seem to accumulate on the graphene surface as soon as graphene is exposed to ambient conditions.[73]

An alternative route to obtain high quality graphene is its direct growth on silicon carbide (SiC). The advantage of graphene on SiC is that large area graphene is available directly on an insulating substrate, at the cost of step edges in the substrate.[74,75] Recent research suggests, however, that it is possible to transfer charge from the SiC substrate to the graphene.[76–78]

III. GRAPHENE EDGES WITHOUT DISORDER

The smaller the graphene nanostructure is, the larger is the influence of the edges compared to the bulk. Similar to carbon nanotubes where the chirality determines the band structure,[79] the edge chirality of graphene nanoribbons determines whether a ribbon is semiconducting or metallic. Section III provides a brief overview on some aspects of periodic graphene edges from a theoretical and experimental point of view. For a more detailed review of graphene edges, see Ref. 80.

A. Zig-zag and armchair edges

The majority of theoretical research was conducted for graphene nanoribbons with perfect zig-zag or armchair edges. For perfect zig-zag nanoribbons, conducting edge states were predicted.[24,81] Armchair ribbons should not support such edge states but exhibit a width-dependent band gap.[24] For ribbons that do not follow the principal crystal directions, a succession of armchair and zig-zag segments was suggested: if there is a sufficient number of consecutive zig-zag segments and the ribbon is narrow enough, an edge state should still survive.[24] Most of these results were obtained using a zone-folding technique,[24] similar to the band structure calculations of carbon nanotubes.[82] Calculations were also performed for nanoribbons where all the dangling bonds at the edges were terminated by hydrogen.[82,83] For armchair ribbons wider than 1.5 nm, the termination by hydrogen does not significantly influence transport.[83] In contrast, for zig-zag nanoribbons, hydrogen passivation of dangling bonds should lead to the opening of a band gap.[84]

B. Reconstructed edges

Even if the edge is oriented along the armchair or the zig-zag crystal direction, the outermost carbon atoms do not necessarily need to follow zig-zag or armchair configurations. The simplest deviations are changes in bond lengths[85] and out-of-plane rippling.[86,87] More complicated reconstructions show a change in the number of carbon atoms in the outermost rings.[85,88–92] A small selection of such edge reconstructions with a changed number of carbon atoms per ring is shown in Fig. 6. Depending on the conditions, such reconfigured edge structures can be energetically more stable than, for example, zig-zag edges.[85] Reconstructed edges where the outermost carbon atoms are passivated by hydrogen were further investigated.[88] Many of these edge configurations have similar energies[85,88,90,92] such that it is hard to predict which type of edge will be prevalent in experiments. It is therefore likely that different fabrication techniques will result in different edges.

C. Functionalization of edges

Due to the broken sp^2 bonds at the graphene edge, carbon atoms missing a partner should be chemically reactive. Theoretically, the termination of the edges with different atoms or molecules was investigated.[93–96] There is also some limited experimental progress in chemically functionalizing the graphene edges.[97–99] It is intriguing that despite the theoretical high chemical reactivity of graphene edges and the huge number of possible molecules that could be attached, little experimental data are available.

IV. MODELING DISORDERED GRAPHENE EDGES

As it is experimentally challenging to fabricate disorder-free graphene edges (see also Sections V and VI), this section discusses theoretical approaches to model disordered graphene edges. These theoretical expectations are then later compared with experimental findings.

A. Removing random carbon atoms at the edge

The majority of disordered edges considered theoretically are perfect armchair or zig-zag ribbons where the outermost atoms are removed.[82,100–108] The details about

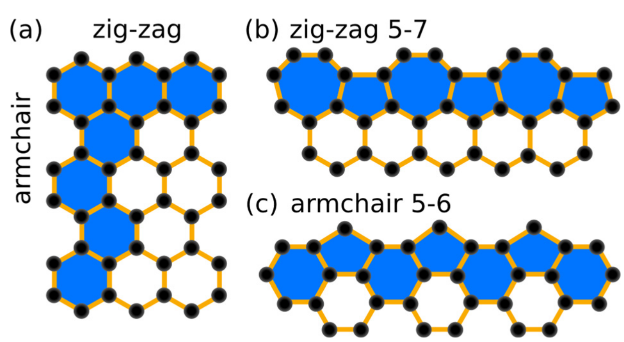

FIG. 6. (a) Zig-zag and armchair edge. (b) Zig-zag 5-7 edge reconstruction. (c) Armchair 5-6 edge reconstruction.

TABLE I. Summary of different theoretical approaches for simulating graphene nanoribbons including assumptions on (a) contacts and periodicity as well as (b) disordered edges.

(a) Contacts	**Refs.**
Infinitely long ribbons or a periodic repetition of ribbon segments	24, 83, 85, 88–92, 95, 104, and 107–109
Finite length ribbons with infinitely extended perfect ribbons as contacts	82, 100–103, 105, 106, and 110–114
Graphene contacts of different widths than the ribbon itself	115–122
Other procedures	123–125
(b) Disordered edges	**Refs.**
Single, double or triple vacancies	102
Removal of random H-C-C-H groups at the edge	82 and 100
Removal of random carbon atoms at the edge	101, 104, and 105
Removal of random carbon atoms at the edge and successive removal of all not double-bound carbon atoms	106
Removal of random carbon atoms not only at the edge but also close to the edge (no holes)	103, 107, and 108

assumptions for contacts/periodicity and methods of removing carbon atoms are summarized in Table I.

For sufficiently narrow nanoribbons with perfect zig-zag or armchair edges, quantized conductance is expected as schematically depicted in Fig. 7. All studies agree that the expected quantization of conductance for nanoribbons with non-perfect armchair or zig-zag edges disappears.[82,100–108]

It is commonly agreed that the conductance generally decreases for ribbons with non-perfect edges[82,100–103,106,107]—except for semiconducting armchair ribbons around the charge neutrality point where conductance is expected to be zero and changes therefore increase the conductance.[100,101] The reasons for this behavior are enhanced backscattering of charge carriers,[82,100,101,105,106] Anderson localization,[100,102,103,105–108] nearest neighbor hopping,[104] and variable range hopping.[104] Several studies found localized states along the disordered edge of the ribbon[103,104,107] and some attributed them to zig-zag segments.[82,108] Fig. 8 shows some results from Ref. 103.

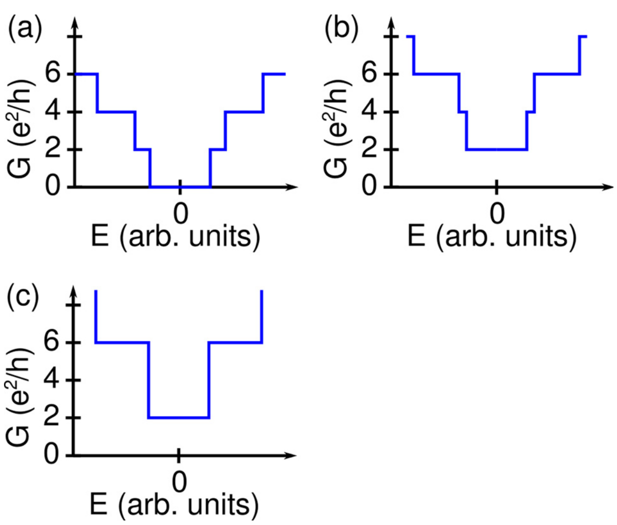

FIG. 7. Schematic conductance as a function of energy of: (a) semiconducting armchair nanoribbon,[100] (b) metallic armchair nanoribbon,[82] and (c) metallic zig-zag nanoribbon.[102]

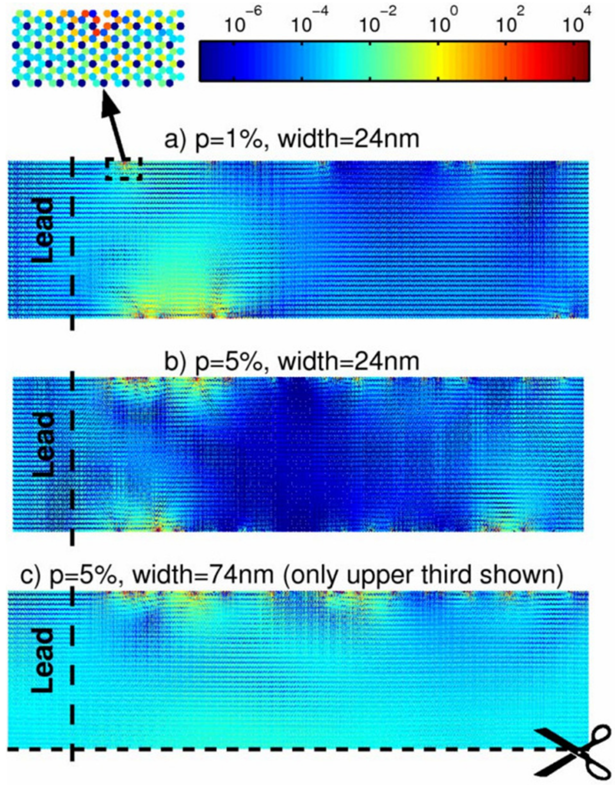

FIG. 8. LDOS calculated for an infinite armchair nanoribbon by Evaldsson *et al.*[103] (a) Width of 24 nm and defect probabilities of $p = 1\%$ and (b) $p = 5\%$. (c) Wide ribbon (74 nm) with defect probability $p = 5\%$. In all three cases, states with enhanced LDOS are found at the edges around defects. Reprinted with permission from Evaldsson *et al.*, Phys. Rev. B **78**, 161407(R) (2008). Copyright 2008 the American Physical Society.

Generally, zig-zag nanoribbons seem to be less sensitive to the removal of edge groups than armchair ribbons. Zig-zag ribbons of nearly identical width have similar band structures as opposed to armchair ribbons where a slight change in width strongly changes the band structure.[82] This difference becomes negligible if defects along the edge are not limited to the outermost row of carbon atoms.[107] In general, the influence of edge defects is found to decrease with increasing ribbon width.[100–103,106,107]

For bilayer graphene with randomly missing edge atoms in both layers, similar results as for single layer graphene are found with the difference that the localization length inside the blocked regime is found to be longer.[111]

Slightly different to the approaches discussed so far is the model from Sols *et al.*[123] which suggests that charge localization and therefore Coulomb blockade can occur due to edge roughness forming "bottlenecks" for transport channels.

B. Other types of simulated edge disorder

Other types of defective edges were studied. Ribbons built of perfect ribbon segments with different widths[104,113] were found to show Anderson localization.[113]

If the width of perfect armchair/zig-zag ribbons is gradually changed very slowly, quantized conductance is expected to still be visible despite being smoothed out.[112]

Further, weak scatterers were introduced by changing the on-site potential of carbon atoms at the edge: they were found to only play a significant role if they are strong enough to lead to Anderson localization.[102]

Additionally, long-range disorder—where the disorder length is much larger than the C–C bond length—was investigated and found to only have a small influence around the Dirac point.[82]

C. Other non-idealities

The influence of metal contacts on the conductance of nanoribbons was investigated.[108,124] Strong changes of the nanoribbon properties close to the contacts[124] as well as generally decreased conductance[108] and asymmetries between electrons and holes[108] were found.

Another class of defects are missing atoms in the bulk which lead to a significant reduction of conductivity due to intravalley scattering.[121] It was further shown that lattice deformations can result in charge localization.[114]

Finally, it was shown that the quantum capacitance of ribbons[126] can strongly alter the geometrically expected capacitance around the Dirac point when side gates are present.[109]

V. EXPERIMENTAL INVESTIGATION OF EDGES

It is challenging to obtain experimental information about the microscopic morphology of the edges. Experimental information on the edges would, however, be extremely useful to compare theoretical predictions with the experimental findings. Some limited information can be obtained by Raman spectroscopy,[127–134] as, for example, perfect zig-zag edges will not result in a D-peak.[135] The other two possibilities to investigate graphene edges are transmission electron microscopy (TEM) and scanning tunneling microscopy (STM). In order to study graphene edges by TEM,[46,133,136–144] the graphene needs to be suspended. Also, imaging by TEM can change the investigated graphene due to the high energy of the employed electrons.[136,142,145] Various edge configurations were found with TEM studies as, for example, shown in Fig. 9.

Alternatively, STM can be employed to image the graphene edges. In order to perform STM on graphene edges, conductive substrates (or a combined SFM/STM mode) as well as especially clean graphene devices are required. While hexagons in the graphene bulk can easily be imaged, the resolution often drops towards the edge such that single atoms cannot be resolved anymore.[146–149] Under special conditions, hydrogenated zig-zag, armchair, and mixed edges were observed.[125,149–153] Recently, also SFM scans of graphene edges were shown.[125]

For multilayer graphene flakes, it is further possible that the edges of several layers fuse together and create so-called "closed edges."[140,154,155]

VI. FABRICATION OF GRAPHENE NANORIBBONS

It is likely that the edge morphology of graphene nanoribbons will depend on the employed fabrication technique. As discussed before, the edge morphology has an important

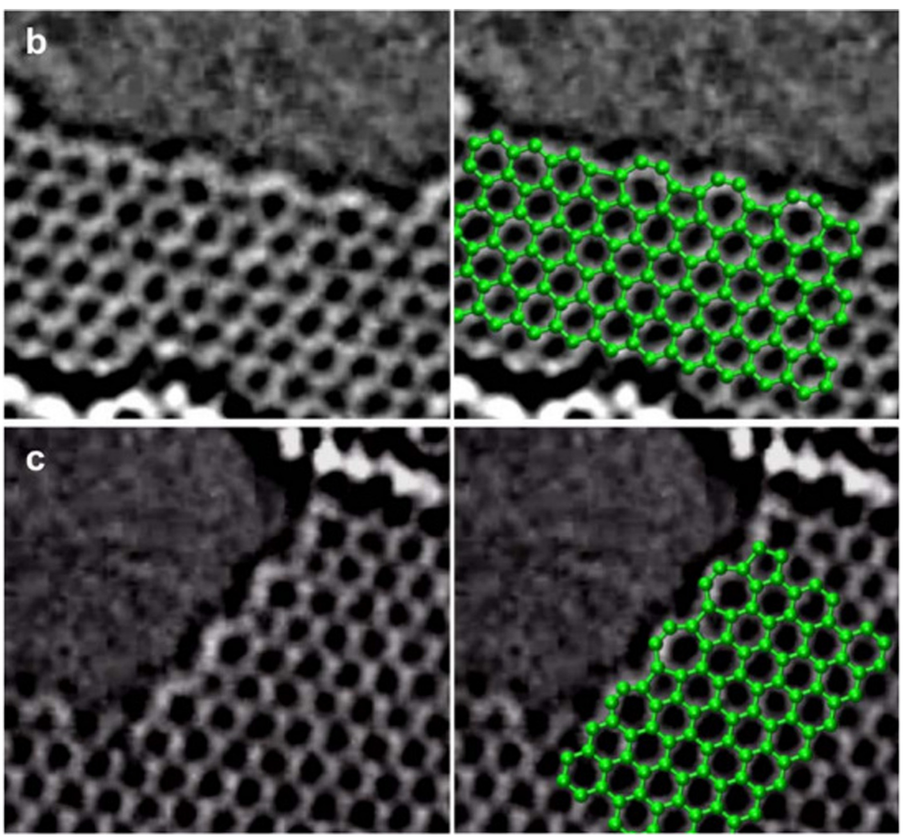

FIG. 9. TEM image of reconstructed 5-7 zig-zag graphene edges from Ref. 139. Reprinted with permission from Koskinen *et al.*, Phys. Rev. B **80**, 073401 (2009). Copyright 2009 the American Physical Society.

impact on transport properties of graphene nanodevices. Similarly, bulk properties such as defects or fabrication residues might depend on the employed patterning method. In experiments, widely different approaches for fabricating nanoribbons were used. An overview of different fabrication techniques for graphene nanoribbons is provided in Table II.

As details provided about the fabrication are often sparse, several of the devices listed as "oxygen plasma" might, for example, have been fabricated with an "oxygen plasma" RIE process. This lack of details in the publications makes a comparison of fabrication processes challenging.

Some of the fabrication techniques (e.g., RIE) allow to fabricate nanostructures of any shape as long as the lithography process provides enough resolution. Others only allow the fabrication of specific geometries (e.g., unzipping of carbon nanotubes). From the etching techniques, some are isotropic (e.g., RIE, all exposed graphene is etched equally fast) and others are anisotropic (e.g., hydrogen plasma etching, graphene close to defects is etched faster). Using these different fabrication techniques, ribbons of different length and width were fabricated.

Just as the patterning technique, the employed graphene/carbon source might have an impact on electronic transport in the graphene nanodevices. Different graphene/carbon sources will likely result in bulk graphene with different microscopic properties, such as, for example, number and type of defects. Table II provides a summary of the different carbon sources that were used to fabricate graphene devices. Many of the references do not explicitly state the graphene source that was used but write, e.g., "mechanical exfoliation." For these cases, it was assumed that the graphene source was natural graphite.

As discussed before, the substrate used for graphene devices can have a significant impact on device performance. A list of substrates used for electronical transport experiments in graphene nanoribbons is provided in Table II.

Finally, as the band structure of graphene depends strongly on the number of layers, it could be expected that the electronical transport properties of graphene nanoribbons also depend on the number of layers. Electronical transport experiments were performed on graphene nanoribbon devices with a different number of layers as summarized in Table II. Again, the information provided about the number of layers is often limited. Many references do not explicitly state how many layers their devices consist of or how this amount of layers was determined. If information is provided, often only an estimate with a large error bar of the amount of layers (e.g., an SFM step height) is reported. When nothing explicitly was stated (i.e., "graphene nanoribbon"), it was assumed that the devices were single layer.

A. Comparison of fabrication techniques

From the different approaches of patterning graphene nanoribbons, one could expect to obtain valuable information on the involved electronical transport processes by comparing data of different ribbons. Comparing nanoribbons fabricated with different processes is, however, difficult: in addition to the limited information, difficulties arise as different references provide different subsets of measurement data. Moreover, there are many possible combinations of how devices can be fabricated: different patterning methods, graphene sources, substrates, number of layers, and fabrication details. A direct comparison is only meaningful if one parameter at a time is changed or if the resulting transport properties are sufficiently different from other devices (discussed in Sec. VIII). In the following cases, a single parameter was changed in the fabrication process.

1. Crystal orientation

For oxygen plasma etched ribbons, transport of several devices on one flake having different angles with respect to each other was investigated. While the exact orientation relative to the crystal lattice was not known, different ribbon edges will on average have a different orientation relative to the graphene lattice. No significant difference in transport was found between the devices.[157]

2. RIE gas

Using the same fabrication process, graphene ribbons were once etched with argon plasma RIE and once with oxygen plasma RIE. Raman measurements indicate that oxygen plasma induces significantly more defects along the edges than argon plasma. The oxygen plasma RIE etched ribbons also showed a much higher variation between devices in transport experiments.[192]

3. Directed and undirected plasma etching

Graphene nanoribbons were patterned once with an undirected plasma process (oxygen plasma ashing) and compared to ribbons patterned with a directed process (oxygen and argon RIE). It was found that devices patterned with the undirected process resulted in significantly more noisy devices.[181]

These findings suggest that seemingly small differences in fabrication processes can have an impact on device performance.

VII. FABRICATION OF GRAPHENE QUANTUM DOTS

Similar to the graphene nanoribbon devices presented in Section VI, fabrication processes are compared for graphene quantum dots. As the fabrication of island geometries is more challenging than the fabrication of simple nanoribbons, the number of employed fabrication techniques is smaller as shown in Table III.

Most of the devices were fabricated on a SiO_2 substrate with the exception of Refs. 61, 240, and 241, where devices were suspended, and Refs. 234, 242, and 243, where devices were fabricated on a hBN substrate. Devices fabricated on hBN were suggested to be "more stable," to show a more regular behavior and to exhibit less disorder.[242,243] Similar to the nanoribbons, devices with different numbers of graphene layers were fabricated as shown in Table III.

TABLE II. Summary of different graphene nanoribbon experiments presented in literature. Experiments sorted by (a) fabrication technique, (b) employed graphite/carbon source, (c) substrate, and (d) the number of graphene layers.

(a) Patterning method	**Nanoribbon experiments in Refs.**
Oxygen plasma	132 and 156–181
Oxygen plasma RIE	182–193
Argon plasma	160 and 194–196
Argon plasma RIE	192
Argon + oxygen plasma	197–199
Argon + oxygen plasma RIE	96, 131, 181, and 200–210
RIE without details about gas	211
Hydrogen plasma	134 and 148
Solution based chemical processes	212–214
Unzipping carbon nanotubes by argon plasma	215
Chemical unzipping of carbon nanotubes	46, 133, 144, 152, 171, and 216–221
Bottom-up fabrication from molecules	151 and 222–226
Chemical etching at high temperature	227
Joule heating	56, 62, 145, 218, and 219
SiC step edges	228 and 229
Oxidation by AFM	230
Natural exfoliation	159 and 231
Helium ion beam	232 and 233
TEM sculpting	145
Electrostatic gating	61 and 234
Others	153 and 235–239
(b) Carbon source	**Nanoribbon experiments in Refs.**
Natural graphite exfoliated	62, 96, 131, 157, 159, 160, 163, 163, 165–175, 178, 181–184, 186, 189, 190, 195–207, 209, 210, 227, 231, 232, and 234
HOPG exfoliated	56, 61, 148, 156, 177, 208, and 235
Kish graphite exfoliated	132, 148, 161, 211, and 230
SiC graphene	179, 180, 188, 228, and 229
CVD graphene	145, 176, 187, 191–193, 233, and 239
Commercial expandable graphite	212–214
Carbon nanotubes	46, 133, 144, 152, 171, and 215–221
Direct CVD growth by nickel replacement	238
(c) Substrate	**Nanoribbon experiments in Refs.**
Amorphous SiO_2	46, 96, 131, 132, 144, 148, 156–163, 165–171, 173–178, 181–184, 186, 187, 189–193, 195, 197–204, 206–208, 210–216, 220, 221, 227, 230, 231, 233, and 239
No substrate (“suspended”)	56, 61, 62, 145, 218, 219, 232, and 238
hBN	192, 205, 209, and 234
$SrTiO_3$	172
SiC	179, 180, 188, 228, and 229
(d) Number of graphene layers	**Nanoribbon experiments in Refs.**
Single layer	46, 56, 62, 96, 131, 132, 144, 145, 148, 156–160, 162, 163, 163, 165–173, 175–177, 179–184, 186–190, 192, 193, 195–206, 208–212, 214–216, 218–221, 227–233, 238, and 239
Bilayer	46, 61, 132, 144, 145, 167, 178, 183, 207, 213, 215, 219, and 234
Multilayer	145, 161, 167, 215, and 219

A. Device geometries

Devices were patterned using different designs with the aim of achieving a certain functionality. This makes a comparison of devices and fabrication processes even harder than for nanoribbons. The majority of devices were fabricated by connecting graphene islands with narrow constrictions to graphene leads.[40,221,242–252,254–273,276–278] Various designs also used gated regions: top gates on a single layer ribbon[253] and split gates on bilayer graphene.[61,234,274] Other designs used a single constriction as a quantum dot[240,241,275] or high resistive contacts.[279]

Patterns were designed with the aim of fabricating single[40,61,234,240–249,251,252,258–260,263,265–268,271,274–279] or serial double quantum dots.[221,250,253–255,257,261,262,264,267,269,270,272,273] Further, more exotic devices with three leads[45,265] or parallel double quantum dots[257,262] were fabricated.

Most devices employed a back gate (see Refs. 40, 45, 61, 221, 234, 240–272, and 275–279]) and one (see Refs. 251, 256, and 271) or multiple (see Refs. 40, 45, 61, 221, 234, 242–250, 252, 254, 255, 257–270, 272, 273, 276, and 278) side gates. Side gates were fabricated with graphene except in one experiment where metal side gates were used.[221] A few designs also used one[263] or multiple top gates.[61,234,253,274] Some devices additionally included a ribbon or SET nearby as a charge detector.[244,258,266–268,271]

VIII. ELECTRONIC TRANSPORT EXPERIMENTS IN GRAPHENE NANORIBBONS

This section presents the findings from electronical transport experiments in graphene nanoribbons. Different interpretations of similar findings in comparable devices are highlighted. Further, the current understanding of physical transport mechanisms is discussed in detail, focusing on etched graphene nanoribbons which comprise the majority of the experiments. Focus is put on the mechanisms leading to charge localization. Finally, transport properties of

TABLE III. Summary of different graphene quantum dot experiments presented in literature. Experiments sorted by (a) fabrication technique and (b) the number of graphene layers.

(a) Patterning method	**Quantum dot experiments in Refs.**
Argon + oxygen RIE	40, 45, 221, and 241–268
Oxygen RIE	269–273
Definition by patterned top gates	61, 234, 253, and 274
Current annealing	240 and 275
AFM oxidation	276 and 277
Oxygen plasma	278
Chemical exfoliation	279
(b) Number of graphene layers	**Quantum dot experiments in Refs.**
Single layer graphene	45, 221, 240, 242–244, 246–257, 259, 260, 262, 265–268, 271–273, and 276–278
Bilayer graphene	40, 61, 234, 258, 261–264, and 274
Multilayer graphene	241, 245, 269, 270, 275, and 279

graphene nanoribbons showing distinctly different properties from the majority of experiments are discussed to highlight limitations of the current transport models and future opportunities.

A. Suppressed conductance

Despite the many different routes taken for fabricating devices, electronic transport properties are very similar for many different graphene nanoribbons. From all references presenting data at low temperature over a large range of charge carrier densities (see Refs. 46, 56, 61, 62, 96, 156–160, 162, 164–166, 168, 173, 174, 176, 180, 186–189, 191, 194–206, 210, 211, 213, 217–219, 227, 229, 233, and 237), most agree that for sufficiently narrow ribbons at sufficiently low temperatures, transport is strongly suppressed. Typically, the conductance decreases with increasing gate voltage until at a certain point conductance is nearly completely suppressed. A further increase in gate voltage then usually results in an increase of conductance. The minimum of the conductance is generally attributed to be roughly at the position of the charge neutrality point. The change of conductance with gate voltage is typically strongly non-monotonic. Such a measurement curve is shown in Fig. 10(a).

Exceptions where the suppression of conductance described above was not observed are Refs. 56, 61, 228, and 234 where a fundamentally different behavior was found. They will be discussed separately at the end of this section.

B. Observation of Coulomb blockade

From those experiments where the conductance was measured as a function of applied bias and gate voltage at low temperature, nearly all observed Coulomb blockade (see Refs. 46, 62, 96, 158, 160, 162, 164–166, 174, 176, 186, 195, 196, 199–206, 230, and 238) with exception of the previously highlighted experiments and Refs. 157, 187, and 211 that did not provide sufficiently high resolution data to make a clear statement. For more details about Coulomb blockade see, e.g., Refs. 280–285. Fig. 10(b) shows Coulomb blockade diamonds recorded in the regime of suppressed conductance from Fig. 10(a), and Fig. 11 shows Coulomb blockade diamonds measured in ribbons fabricated with different techniques.

In many of these experiments, the presence of multiple dots in series was inferred from the observation of overlapping Coulomb diamonds.[96,160,162,165,186,195,200–203,205,238] Additional top gates[158,160,166,169,170,178] or side gates[96,162,200,201] were fabricated in order to obtain more information about the extent, location, and number of "quantum dots" that form inside the ribbon. Note that the term "quantum dot" is used in this context to describe the rather stochastic Coulomb blockade observed in graphene nanoribbons, rather than a system with a well defined island where charge is added. By using additional gates, it was confirmed that several quantum dots coexist in longer devices,[162] and a change in the position of different quantum dots as a function of energy was found.[201] Scanning gate

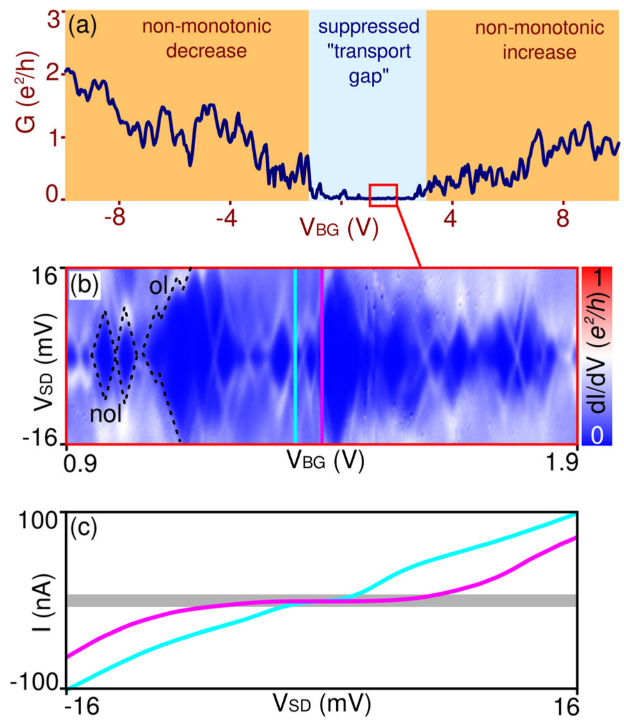

FIG. 10. (a) Typical low temperature conductance of a graphene nanoribbon as a function of applied back gate voltage: the conductance of the order of e^2/h or larger decreases non-monotonically, reaches a region where it is strongly suppressed, and then increases again non-monotonically. (b) Bias dependence of the current recorded in the region marked with a red box. In order to enhance the visibility, the differential conductance dI/dV_{SD} is plotted. Non-overlapping (nol) and overlapping (ol) Coulomb diamonds are visible. (c) Current as a function of applied bias voltage at the two positions marked with cyan and magenta. The current increases about linearly outside of the blocked regime indicating that the device is in a multilevel regime. Ribbon on hBN (device #2 from Ref. 205) with a length of 240 nm and a width of 80 nm.

measurements confirmed both the presence of multiple quantum dots in the ribbon as well as their changing position with energy.[206]

A detailed investigation of the Coulomb blockade diamonds resulted in additional insights. The addition of single electrons to the ribbon was demonstrated using a nearby SET.[201] It was further excluded that the observed features stem from resonant tunneling or Fabry-Pérot interferences.[162] Also, influences of cotunneling were observed.[46,162]

C. Models explaining Coulomb blockade

A number of models were suggested to explain the observed suppression of conductance and the quantum dot-like behavior at low temperatures.

The earliest publications suggested that the band gap theoretically calculated for narrow armchair ribbons (as discussed before, zig-zag ribbons do not exhibit a band gap) was the cause of the suppressed conductance.[156,157] This model has obvious limitations as a band gap alone cannot explain Coulomb blockade.

The model with the band gap was extended into microscopic graphene islands separated by smaller graphene parts that exhibit a band gap.[158] Along similar lines, electron-hole

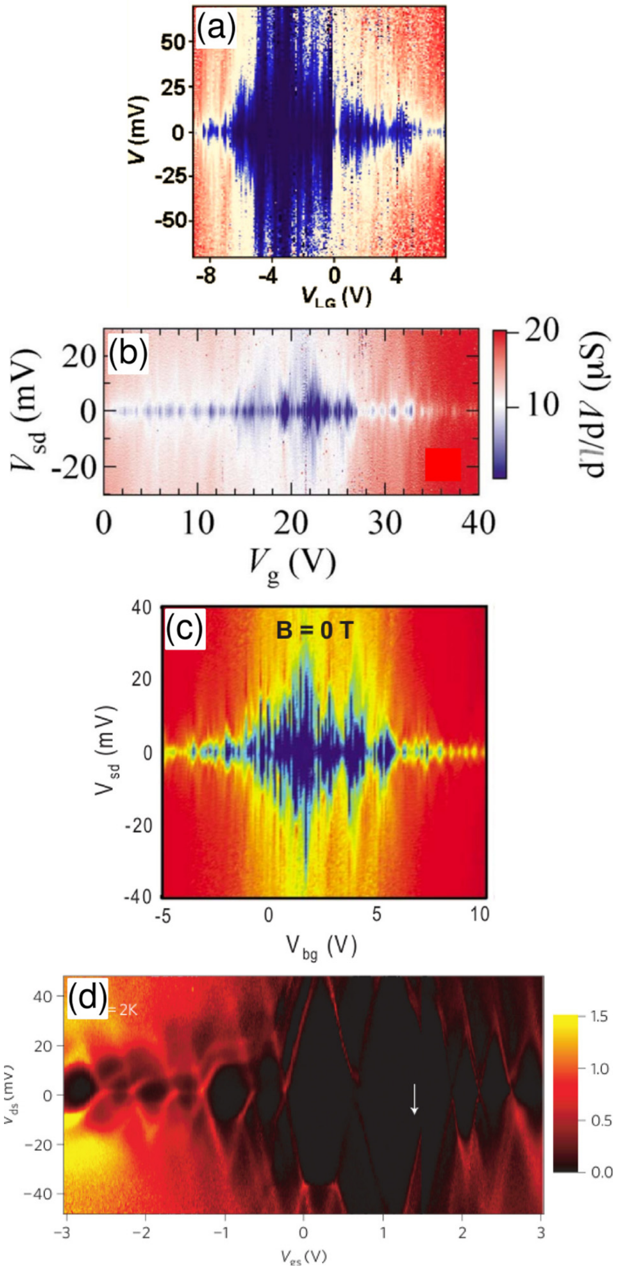

FIG. 11. Coulomb blockade observed in different experiments: devices fabricated by (a) oxygen plasma etching,[158] (b) AFM oxidation lithography,[230] (c) argon plasma etching,[195] and (d) chemical unzipping of carbon nanotubes.[46] (a) Reprinted with permission from Appl. Phys. Lett. **91**, 192107 (2007). Copyright 2007 AIP Publishing LLC. (b) Reprinted with permission from Appl. Phys. Lett. **94**, 082107 (2009). Copyright 2009 AIP Publishing LLC. (c) Reprinted with permission from Oostinga *et al.*, Phys. Rev. B **81**, 193408 (2010). Copyright 2010 the American Physical Society. (d) Reprinted with permission from Wang *et al.*, Nat. Nanotechnol. **6**, 563–567 (2011). Copyright 2011 Macmillan Publishers Ltd.

puddles were suggested to be the cause for the quantum dots.[159] Tunneling between different dots would then occur through regions with a band gap (percolation).[159] This model was further adapted into a model where the band gap was replaced by an energy gap[286] due to quantum confinement.[162,165,186,201,202] The presence of an energy/band gap is crucial for these models to ensure that Klein tunneling is replaced by conventional tunneling.[201] Temperature dependent measurements established that transport can be described by variable range hopping[195,196] or alternatively a combination of variable range hopping, thermally excited hopping, and a Coulomb gap.[166,238] Further variations of this model were suggested.[199,203]

D. Band gap

In contrast to attributing the suppressed conductance to charge localization, a large number of references suggest that a band gap is the origin of the suppressed conductance observed in experiment (see Refs. 46, 144, 148, 156–158, 163, 168, 180, 182, 183, 187, 188, 192, 212, 213, 215, 218–220, 227, 228, and 231—the authors of Refs. 157 and 158 updated their interpretation in later publications as more data became available[166]). While a "band gap" is a material and geometrical property, an energy gap originating from Coulomb blockade arises due to electron-electron interaction in combination with the random localization of charge carriers. A separate section in Appendix A of this review highlights what the authors of this review assume when using the term "band gap." As for various applications it is important to obtain a real band gap, the different interpretations are compared in the following. The experiments attributing the suppressed conductance to a band gap fall in one of two groups: either no low temperature data were recorded[148,163,183,212,213,227] or no data suitable to observe Coulomb blockade diamonds were presented.[144,156,168,180,182,187,188,192,218–220] Two notable exceptions are Refs. 46 and 228 which will be discussed separately. Without further data, it is hard to determine if the random localization of charge carriers can be excluded as being the main mechanism for the observation of suppressed conductance in those experiments. It is, however, important to note that so far no experiment exists that clearly rules out the possibility of an energy gap due to quantum confinement in graphene nanoribbons.

E. Charging energy and area of localized charge

Several experiments (in graphene nanoribbons[205,209] and quantum dots[40]) allowed to compare the self capacitance of a site of localized charge to the capacitances to the different gates. The self capacitance is the sum of all capacitances from an object to its surroundings. It was found that the largest contributions to the self capacitance originate from coupling to neighboring states of localized charge and from coupling to the leads. This behavior is sketched in Fig. 12.

The size of a Coulomb diamond in bias direction (i.e., the "charging energy") is determined by the self capacitance for a single dot, if the area on which charge is localized is rather large. For smaller dots, additional contributions due to quantum confinement can play a role. The charging energy is further enhanced by capacitive coupling to neighboring dots for multidot systems.[285] This strong dependence of the charging energy on details of the coupling strength to neighboring states makes it therefore extremely challenging to extract areas on which charge is localized.

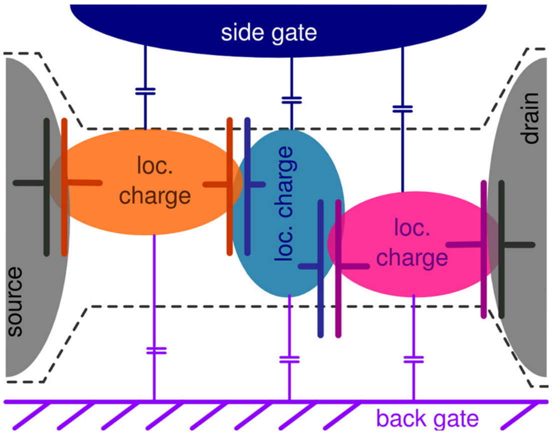

FIG. 12. For graphene nanostructures with side gates and a back gate (separated by 285 nm SiO_2), the self capacitance of a site of localized charge is to a large part given by the coupling capacitance to the neighboring sites of localized charge and to the leads. Capacitances to side gates and the back gate are typically much smaller. The coupling originates likely from a wave function overlap between different sites of localized charge and the leads. This is similar to double quantum dot experiments where the wave function overlap between the two dots is changed by a barrier gate between the dots.[285]

F. Transport gap, back-gate gap, and source-drain gap

To more quantitatively interpret and compare the measured data, the empirical term "transport gap" was introduced, describing the range in which transport is strongly suppressed: typically, the "source-drain gap" (SDG) and the "back-gate gap" (BGG) were used to describe the relevant ranges.[200] Both values may be considered to be problematic as they are defined differently by different authors and because their physical interpretation is difficult. The size of the SDG mostly characterizes the coupling strength between a site of localized charges and neighboring sites or leads as discussed before. The size of the BGG strongly depends on the exact geometry of the device as it is directly related to the capacitance of the ribbon to the back gate. Oxide thickness, ribbon width, and the presence of side gates, top gates, and electrodes will directly enter this capacitance.

For ribbons of similar geometry, a comparison is meaningful.[96,165,166,200,202,204] It was found that both SDG[96,166,202,204] and BGG[96,200,202] increase for narrower ribbons. This is not surprising by taking into account the discussion from Fig. 4: wide devices do not show any suppressed conductance, whereas narrower devices of the order of 100 nm do. The increase in both BGG and SDG is therefore a logical consequence.

It was further shown that longer ribbons result in higher SDG,[165,166,204] but no clear trend between length and BGG was found.[165] Increasing the length allows the formation of multiple sites of localized charges in series, resulting in a higher source-drain voltage needed to be applied for current to flow. Conversely, the density necessary for the disappearance of (strong) charge localization will not change significantly by making the ribbon longer.

Finally, it was shown that the BGG got smaller and shifted closer to zero back gate voltage upon thermal annealing of the ribbons, but the SDG did not change significantly.[165]

G. Disorder from the edges

There are a number of imperfections that can influence transport in graphene nanodevices and might lead to charge localization. A selection of such imperfections is schematically depicted in Fig. 13. In order to distinguish between disorder originating from the bulk and from the edges, ribbons were fabricated on a hBN substrate and annealed.[205] While for micron sized control devices the quality improved, the transport properties of the nanoribbons on hBN were indistinguishable from their counterparts on SiO_2. Subsequent contamination with PMMA decreased the quality of the control devices but did not significantly influence the nanoribbons. It was therefore concluded that the imperfect edges of reactive ion etched devices are mostly responsible for the observed localization of charge. A direct comparison of devices on SiO_2[203] and on hBN[205] is shown in Fig. 14.

In Ref. 211, the opposite experiment was performed: instead of decreasing bulk disorder, it was increased by evaporating cesium atoms on top of an existing ribbon. As a result, the region of suppressed conductance was shifted to more negative values and transport was generally more suppressed.[211] Similarly, doping with potassium atoms strongly shifted the position of the Dirac point to more negative values.[156] The additional atoms on top transfer electrons to the ribbon and might provide additional scattering centers.

These findings together suggest that bulk disorder plays only a minor role if it is sufficiently weak. Stronger bulk disorder might, however, provide additional sites at which electrons can be trapped and lead to Anderson localization.[102]

It is worth noting that in the experiment from Ref. 192, extremely narrow nanoribbons were etched on both silicon dioxide and hBN substrates as well. The authors demonstrate that devices on hBN show consistently lower currents and much higher on-off ratios than their counterparts on silicon dioxide. The reason for this difference is not understood.

H. Charge localization along the edge

The measurement of short graphene constrictions in Ref. 209 gave evidence that some of the states resulting in

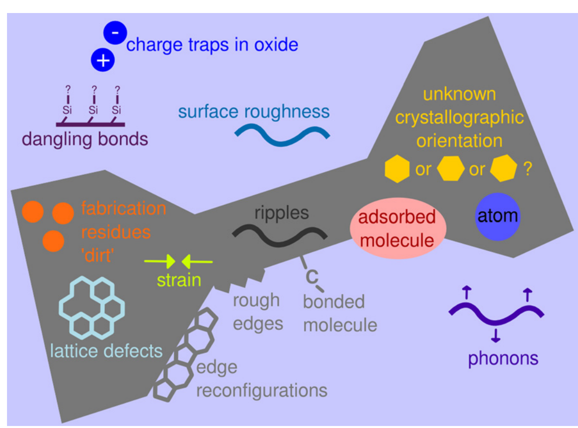

FIG. 13. A number of disorder sources for graphene nanodevices are schematically depicted. The disorder can be grouped into disorder originating due to the presence of edges and disorder originating from substrate, bulk graphene, and contaminations ("bulk disorder").

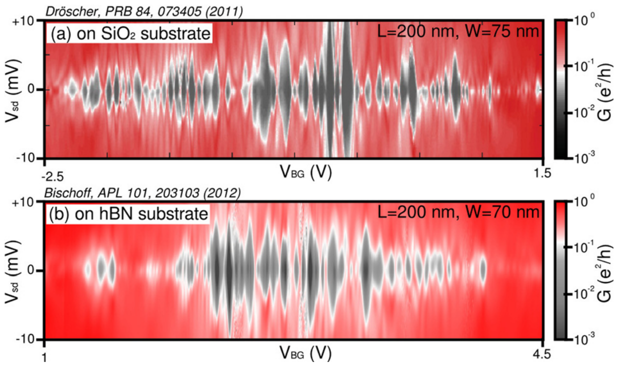

FIG. 14. Direct comparison of the low temperature transport properties of a graphene nanoribbon fabricated on (a) silicon dioxide[203] and (b) on hBN.[205] Aside from microscopic differences, the general transport properties are unchanged. (a) Reprinted with permission from Dröscher *et al.*, Phys. Rev. B **84**, 073405 (2011). Copyright 2011 the American Physical Society. (b) Reprinted with permission from Appl. Phys. Lett. **101**, 203103 (2012). Copyright 2012 AIP Publishing LLC.

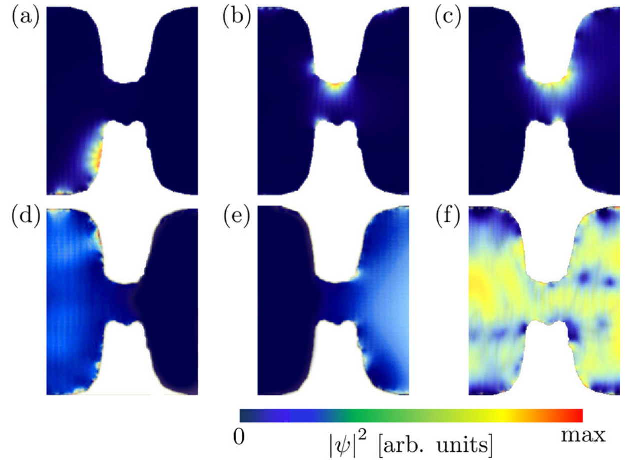

FIG. 15. Wave function envelopes calculated for a 30 nm wide and 30 nm long graphene constriction.[209] No bulk disorder was assumed and edge disorder was introduced by removing random carbon atoms at the edges. Different pictures correspond to different energies. (a) Localized state at the edge of the lead. (b) and (c) Localized states at the edges of the constriction with different extents. (d) and (e) Wave functions delocalized over the leads. (f) Wave function delocalized over the whole device. Reprinted with permission from Bischoff *et al.*, Phys. Rev. B **90**, 115405 (2014). Copyright 2014 the American Physical Society.

Coulomb blockade are localized along the edge of the device. These states are allowed to extend out of the constriction along the edge of the device. A small wave function overlap between these states along the edge and the extended wave functions in the leads are likely responsible for the observation of Coulomb blockade. Such states localized along the edge were also predicted by theory.[103,104,107]

It was further estimated that the length on which electrons are localized along the edge is of the order of 100 nm and therefore significantly longer than the physical disorder length of the edge which is on the nanometer scale. States localized on much shorter lengths might exist but will not be visible in transport as they fail to couple to both leads.

In order to observe Coulomb blockade, transport also needs to be sufficiently suppressed through the bulk of the ribbon. This suppression could be the result of a small density of states and/or additional localized states in the bulk that couple weakly to the leads and the states at the edge.

These findings were qualitatively reproduced with tight-binding calculations where random atoms along the edge were removed. Fig. 15 exemplarily shows a number of localized states that were calculated for disordered edges. It also becomes apparent that only states that manage to couple to both leads will contribute to transport.

While the exact mechanism for charge localization along the edge is not understood in detail, it is assumed that some kind of sufficiently strong disorder at the edge changes the potential landscape such that electrons prefer to be located at the edge rather than in the bulk. As Coulomb blockade was found in many different experiments where devices were fabricated with different processes, the mechanism for the charge localization along the edge does likely not require any specific edge configuration. Due to the large extent of the wave function, the electrons will not be trapped at a single defect site. For higher charge carrier densities, a finite density of states in the bulk might appear such that transport is not governed by localized charges anymore. Fig. 16 schematically depicts this interpretation of the results.

Within this picture, it is easy to explain why wider ribbons ($w > 100$ nm) usually do not feature Coulomb-blockade:[157,166,200,202,204] as there are more electrons located in the bulk per unit edge length, the edge might fail to localize all of them resulting in a finite density of states in the bulk. It is likely that charge carriers will still be localized along the edge but transport is dominated by bulk contributions. Such localized charges along the edge might also explain why in

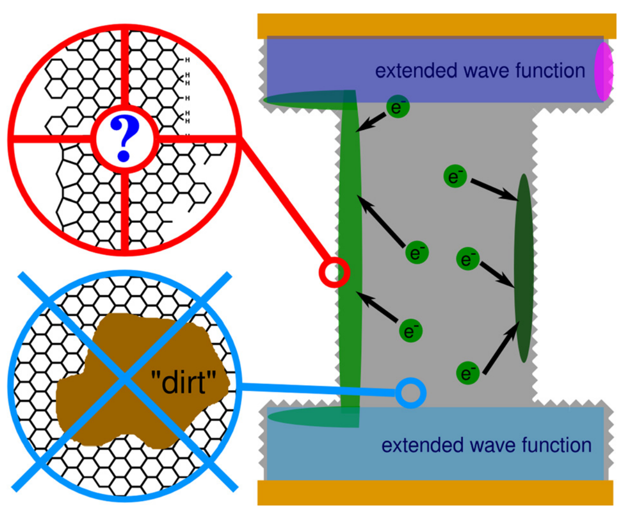

FIG. 16. A nanoribbon (center) is connected via wide graphene leads to two metal contacts. The edges are disordered on a length scale of 1 nm. Electrons in the bulk of the ribbon prefer to be localized at the edges, presumably due to the disorder there. It is generally unknown what the edges look like on a microscopic level. Also, the edges will be different for different experiments. Extended wave functions exist in the wide graphene leads. A state localized along the edge contributes to transport if it manages to connect the two extended wave functions in the leads such as the green state on the left side of the ribbon. The green state on the right side of the ribbon and the magenta state at the edge of the upper graphene lead will, however, not contribute to transport unless they are part of a chain of strongly coupled states that connect the two leads.

graphene ring experiments, the area on which transport happens is generally smaller than the ring width.[32,36]

Recent experiments have shown that also in other experiments localized states in ribbons can be found that are clearly located more towards one side of the ribbon.[181,210]

I. Interference pattern from the leads

In Ref. 209, a clearly visible pattern of additional lines roughly parallel to the diamond edges was observed and explained by phase coherent interferences in the graphene leads adjacent to the nanoconstriction. A zoom of the data presented in Ref. 209 is shown in Fig. 17. Care has therefore to be taken with the identification of lines inside and outside of Coulomb diamonds that resemble electronic excited states. The observation of lines parallel to the diamond edges is consequently not a sufficient criterion for the observation of electronic excited states.

J. Different devices and cooldowns

In order to check the reproducibility, it is worthwhile to fabricate devices of similar geometry and measure each device in several consecutive cooldowns. For the experiments where different devices of similar geometry were investigated, it was found that the transport details depended strongly on the microscopic configuration of the device.[165,205,209] When a device was measured in consecutive cooldowns, transport details changed.[162,205] While some devices were electronically stable over a long period of time in one cooldown, others changed their transport details spontaneously within one cooldown.[205] The general transport features such as the suppressed conductance and the observation of Coulomb blockade were, however, unaffected by those changes. In addition, thermal annealing[165] as well as current annealing[219] were shown to significantly change transport properties.

Based on these findings, different possible mechanisms responsible for the observed changes can be discussed. It is, for example, unlikely that the atomic edge configuration spontaneously changes at cryogenic temperatures. Also, adsorbates ("dirt") will most likely be immobilized at cryogenic temperatures. Factors like surface roughness and crystallographic orientation will even be constant over several cooldowns. Possible spontaneous changes at low temperature could, for example, originate from the charging of defect sites in the substrate or at the edges. Due to the many different nonidealities (selection see Fig. 13) and a lack of systematic experiments, it is currently not possible to successfully correlate all observed changes in transport measurements to a microscopic cause.

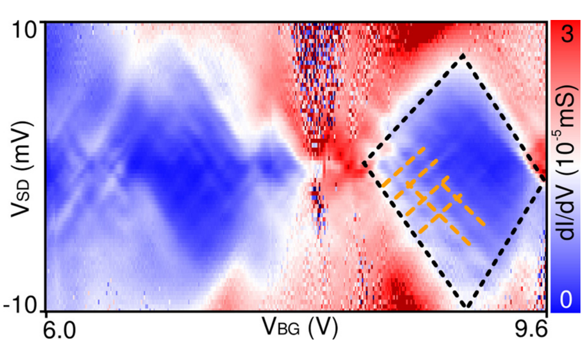

FIG. 17. Zoom of the data presented in Fig. 2(b) of Ref. 209. The measured data can be explained by the overlap of the Coulomb blockade diamonds (black lines) of the constriction and the phase coherent interference pattern from the leads (orange lines).

K. Electronic transport properties different from Coulomb-blockade behavior

There are a number of experiments where the investigated ribbons showed transport behavior clearly different from Coulomb blockade. These experiments give a perspective on the potential transport characteristics that can be obtained by a better control over the microscopic details in graphene nanoribbon devices or by improving the fabrication processes.

1. Quantized conductance

Tombros *et al.*[56] showed a suspended graphene ribbon device that was current annealed. Upon successful annealing, quantized conductance was observed as expected for narrow and ballistic two-dimensional conductors.[287,288] Up to today, it was not possible to reproduce these results suggesting that a very special device geometry and edge arrangement were necessary to obtain quantized conductance. Quantized conductance was also observed in bilayer graphene constrictions that were defined by electrostatic gating ("split gates"): either in suspended graphene[61] or encapsulated in hBN.[234]

2. Silicon carbide step edges

Baringhaus *et al.*[228] showed transport data on graphene ribbons grown on SiC step edges. No signature of Coulomb blockade was observed. While the mechanisms are not yet fully understood, the authors claimed to observe ballistic transport over lengths of microns even at room temperature.[228] More recent work on this topic addressed questions as to where exactly current might be flowing in these devices.[229]

3. Unzipped carbon nanotubes

Most experiments where nanoribbons were fabricated from unzipped carbon nanotubes unfortunately do not provide low temperature transport data as a function of applied gate voltage and bias voltage.[133,144,152,171,215–221] It is therefore not possible to determine if those devices also show Coulomb blockade or not. One notable exception is Ref. 46: the unzipped carbon nanotube with a width of about 20 nm showed extremely clean Coulomb blockade with regular spacing and various other intriguing features resembling "shell filling" and "Kondo effect" (see also Fig. 11(d)). The clarity of the features suggests that there might be some fundamental difference to the other experiments. Additional devices presented in the supplementary of Ref. 46, however, showed transport characteristics similar to other nanoribbons showing less regular Coulomb blockade. One possible explanation is that this specific process of unzipping carbon nanotubes can, under certain conditions, lead to significantly less defective edges.

4. Bottom-up fabrication of nanoribbons

A class of devices that are fundamentally different from most other nanoribbons are the ones obtained by bottom-up fabrication using molecules and resulting in perfect edges.[151,222–226] Unfortunately, it was so far not possible to fabricate sufficiently long devices for transport experiments. Some limited transport data were obtained by lifting a ribbon off the metal surface with an STM tip.[224]

L. Additional investigated parameters

Various different experimental parameters were varied to study graphene nanoribbons. For completeness, a summary is provided here:

1. Magnetic field

Various experiments investigated graphene nanoribbons in perpendicular magnetic field (see Refs. 56, 62, 164, 173, 189, 190, 195, 197, 198, 200, 205, and 214]) and in some of them, quantum Hall effect was observed (see Refs. 62, 189, 197, 198, and 205).

2. Temperature

In a number of experiments, electronic transport as a function of temperature was investigated (see Refs. 46, 156, 157, 166, 168, 174, 182, 187, 188, 192, 195, 203, 205, 211, 212, 214, 218–220, and 238) and most experiments found a suppression of conductance for narrow ribbons and low temperatures.

3. Functionalization

Upon treatment of graphene nanoribbons on SiO_2 with a short HF (hydrofluoric acid) dip, transport was significantly changed:[96] conductance was less suppressed, the BGG shifted towards zero back gate voltage, and the capacitance between side gates and localized states strongly depended on the applied side gate voltages. While details are not fully understood, it was speculated that the HF alters the edge by passivating dangling bonds with fluorine.[96] More insights could be obtained if these experiments were repeated for ribbon devices on hBN as the HF also alters the SiO_2 substrate.

4. Noise

Different references investigated the noise characteristics of graphene nanoribbons.[183,196,199]

5. High current regime

In graphene nanoribbons, currents larger than 1 μA per 1 nm width were applied to the ribbons,[145,171,175,176,194] and it was found that the thermal conductivity of graphene nanoribbons is about one order of magnitude smaller than for bulk graphene, which is attributed to defects and the presence of edges.[171]

IX. ELECTRONIC TRANSPORT EXPERIMENTS IN GRAPHENE QUANTUM DOTS

This chapter focuses on graphene quantum dot experiments that provide additional insight into the physical transport mechanisms discussed in Section VIII. A more thorough review of graphene quantum dots can be found in Ref. 47.

A. More regular Coulomb blockade than in nanoribbons

In most single quantum dot experiments, Coulomb blockade diamonds were observed as depicted in Fig. 18 for the device shown in Fig. 3. Most experiments showed one or several Coulomb diamonds closing at zero bias[40,45,61,234,240,241,243–249,251,252,256,258,260,263,267,268,271,276–278]) and in a few experiments, diamonds did not close.[242,274,275,279]

For the double dot experiments, the expected hexagon patterns were observed[221,250,253–255,257,261,262,264,269,270,272,273] and various references report the observation of finite bias triangles.[250,253–255,261,264,272]

Generally, Coulomb blockade diamonds are much more regular in quantum dot devices than in graphene nanoribbons. This can directly be seen by comparing Fig. 18 with Figs. 10, 11, and 14. Some caution has to be taken because often only a very small number of Coulomb diamonds were shown: the range from $V_{BG} = 0 - 2\,\mathrm{V}$ in Fig. 18 looks, for example, much more regular than the range from $V_{BG} = 2 - 3\,\mathrm{V}$.

B. Influence of constrictions

Taking into account that graphene nanoribbons usually display stochastic Coulomb blockade, it is surprising that graphene islands connected with graphene nanoribbons to graphene leads act as relatively well behaved quantum dots. The influence of the constrictions on transport through graphene quantum dots was discussed in various experiments. Often, it was found that the coupling between a dot and another dot or a lead changed non-monotonically with applied gate voltage.[245,247,250,253,254,258,259,261,262,264,270,276]

Multiple experiments found "transmission resonances"[45,242,245–247,254,258–261,265,268] originating from the constrictions. Most of them were identified by measuring transport as a function of multiple gates.[45,245–247,260,265] The resonances were explained by "localized states" in the constrictions,[45,245,247,256,259,260,265,268] by the appearance of a (transport) gap[246,247] or by "parasitic charge puddles."[221] In other experiments, the constrictions were believed to exhibit

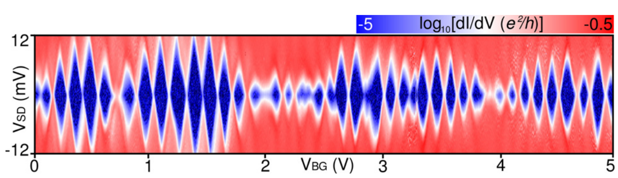

FIG. 18. Coulomb blockade measured in the device presented in Ref. 40 (same device as in Fig. 3) in a different cooldown. Despite measuring many consecutive non-overlapping Coulomb diamonds, the device is clearly in a regime where three dots in series need to be passed by an electron moving from one contact to the other. All side gates are grounded.

a confinement gap[278] or to behave as QPCs.[276] Also, the term "stochastic Coulomb blockade" was used to describe transport in one double dot experiment.[269]

C. Single Coulomb diamonds as a consequence of cotunneling

The measurements of the quantum dot structure from Fig. 3 (Ref. 40) showed that non-overlapping Coulomb diamonds can be observed even when several sites of localized charge are arranged in series. The multiple sites of localized charge were identified and their position was triangulated with the help of multiple side gates. Fig. 19(a) exemplarily shows the current flowing through the device as a function of voltages applied to two different side gates. Three different sets of slopes are clearly visible (yellow dashed lines) indicating that at least three sites of localized charge (or to follow the notation from before: three quantum dots) are present in the device.[285] Using a different set of gates as shown in Fig. 19(b), however, reveals only one set of slopes, which highlights that employing a suitable gate geometry is crucial for locating sites of localized charge. From different gate configurations, the positions of the sites of localized charge inside the graphene structure could be triangulated: one is located in the island and (at least) one each in the two constrictions as schematically depicted in Fig. 19(c).

The system therefore has to be treated as a serial quantum dot. Within this picture, it is surprising that single non-overlapping Coulomb diamonds were measured in the same regime. In order to explain this, higher order tunneling processes over virtual states need to be considered. The situation is schematically depicted in Fig. 20: whenever an energy level of the middle dot in the island is aligned with the leads, a Coulomb peak is measured. The outer two dots are, however, typically in Coulomb blockade such that a second order cotunneling process over a forbidden ("virtual") state is necessary to transport an electron from the lead to the island. As second order cotunneling is generally more probable than third- or fourth-order cotunneling, the middle dot is typically the one that can be linked to the observed Coulomb diamonds.

These findings have immediate consequences: single dot physics (e.g., dot Kondo effect[289]) or double dot physics (e.g., spin blockade[290,291]) cannot easily be investigated in such a system as at least three dots in series are found. This is in stark contrast to, for example, quantum dots in GaAs where tunneling barriers are formed by QPCs and the dots therefore show clear single dot behavior.[292]

As there are various experiments that have found "transmission resonances" originating from the constrictions as well as non-closing Coulomb diamonds in graphene quantum dots, it is therefore likely that this behavior is quite generic for many devices.

It was further found that the site of localized charge in the island is rather stable in size and position, whereas the "quantum dots" in the constrictions change their size as well as their position by applying gate voltages. This suggests that the charge might be homogeneously distributed over the island (compare also supplementary material of Ref. 209)

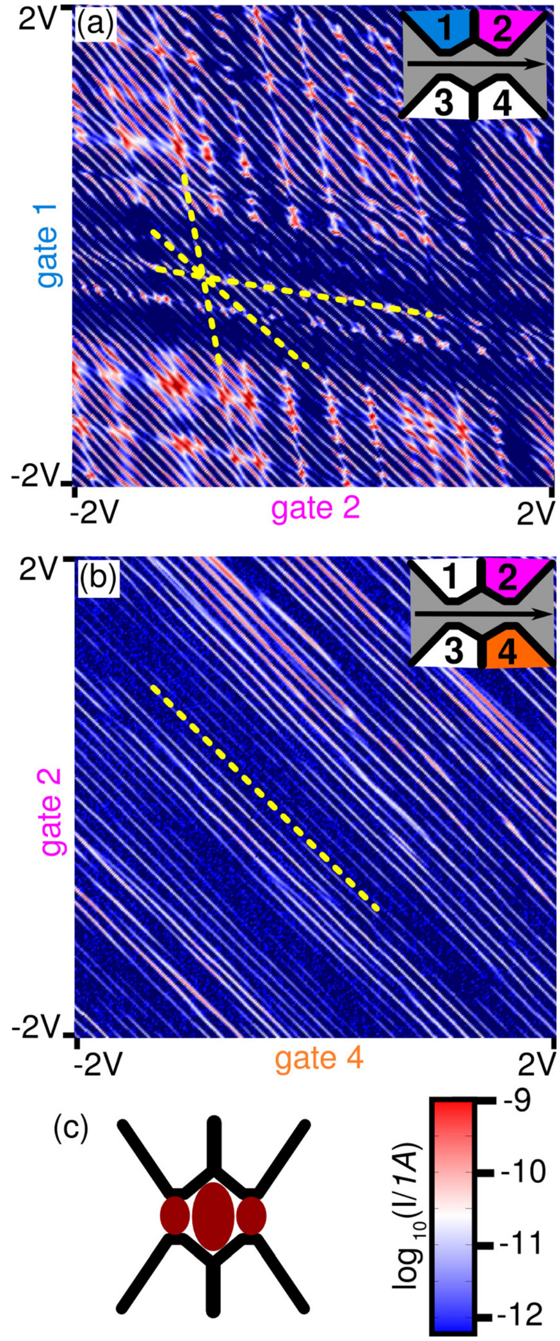

FIG. 19. Current through the dot at a fixed small bias as a function of applied side gate voltages for the device in Fig. 3 (see Ref. 40). For the gate configuration in (a), multiple sets of lines are found, whereas for the gate configuration in (b) only diagonal lines are found. (c) Based on measuring additional gate configurations, three sites of localized charge (i.e., "quantum dots") were identified: one located in each constriction and one in the island. Adapted with permission from Bischoff *et al.*, New J. Phys. **15**, 083029 (2013). Copyright 2013 IOP Publishing.

which would explain why Coulomb blockade is generally more regular in island-shaped devices than in graphene nanoribbons. Further, as nanoribbons often exhibit several localized states in series, it is likely that cotunneling processes are also important in graphene nanoribbons.

Another parameter that was investigated was the capacitive coupling between different sites of localized charge. It was found that whenever different energy levels of the three "quantum dots" are nearly aligned, the size of the Coulomb

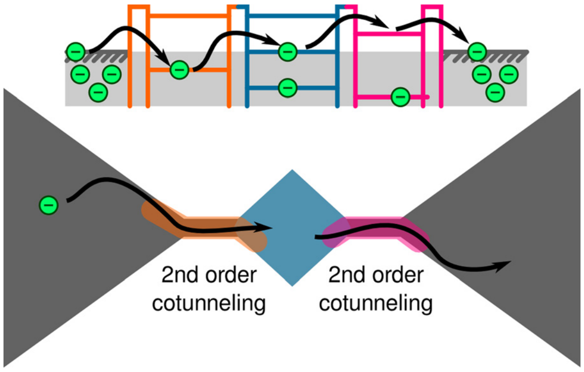

FIG. 20. Schematic diagram of how transport in the quantum dot experiment from Ref. 40 can be interpreted: a Coulomb resonance is measured when an energy level of the island (blue) is aligned with the leads. Strong tunneling coupling of the localized states in the constrictions (orange, magenta) results in second order cotunneling through these states. Higher order tunneling processes occur through virtual states (i.e., electrons travel over levels that are either already occupied or above the Fermi level).

diamond shrinks indicating an enhanced capacitive coupling.[40] This is demonstrated in Fig. 21 for the triple dot device: the charging energy of the island got significantly decreased when one of the levels of the localized states in the constrictions came close to resonance. The width of the diamond, however, stayed constant. It is likely that an increased overlap of the wave functions in the constriction and in the island is responsible for this behavior. This explains why effects such as shell filling[293,294] are hard to observe.

D. Electronic excited states

In a number of single-island graphene devices, features outside but parallel to the Coulomb blockade diamond edge were found and interpreted as electronic excited states.[240,248,249,251,252,267,268,271] Similarly, features parallel to the base line of finite bias triangles in double-island devices were interpreted as electronic excited states[253,254,261,264] or electron phonon coupling.[255] In some cases for the single-island devices, cotunneling lines corresponding to the excited state features were observed inside the Coulomb diamonds.[248,249,251] In Ref. 45, such lines that were parallel to the Coulomb diamond edge were observed, but it was clearly shown that the dot was in a multi-level regime.[295]

There are a variety of other effects that can lead to lines being parallel (or nearly parallel) to the edges of Coulomb diamonds, as, for example, coupled charge traps,[296] electron-phonon coupling,[297] or density of states fluctuations[282,298,299] and interferences[209] in the leads. Similar arguments might not only be true for the leads of the devices but also for the (non-ideal) constrictions.[254] Care has therefore to be taken when interpreting features in conductance as electronic excited states.

E. Magnetic field behavior

Aside from changing gate voltages and applied bias, devices were investigated in parallel[252,261,277] and perpendicular[61,242,243,248,249,251,252,260,267,276,279] magnetic field. The magnetic field was used to probe the electron-hole crossover[248,249] and investigate the Zeeman splitting.[252,277] No preferential spin filling sequence was found.[252,277]

F. Graphene quantum dots beyond electronic transport measurements

There are a number of other approaches for fabricating quantum dots out of graphene. These approaches were so far, however, not used for electronic transport experiments. They

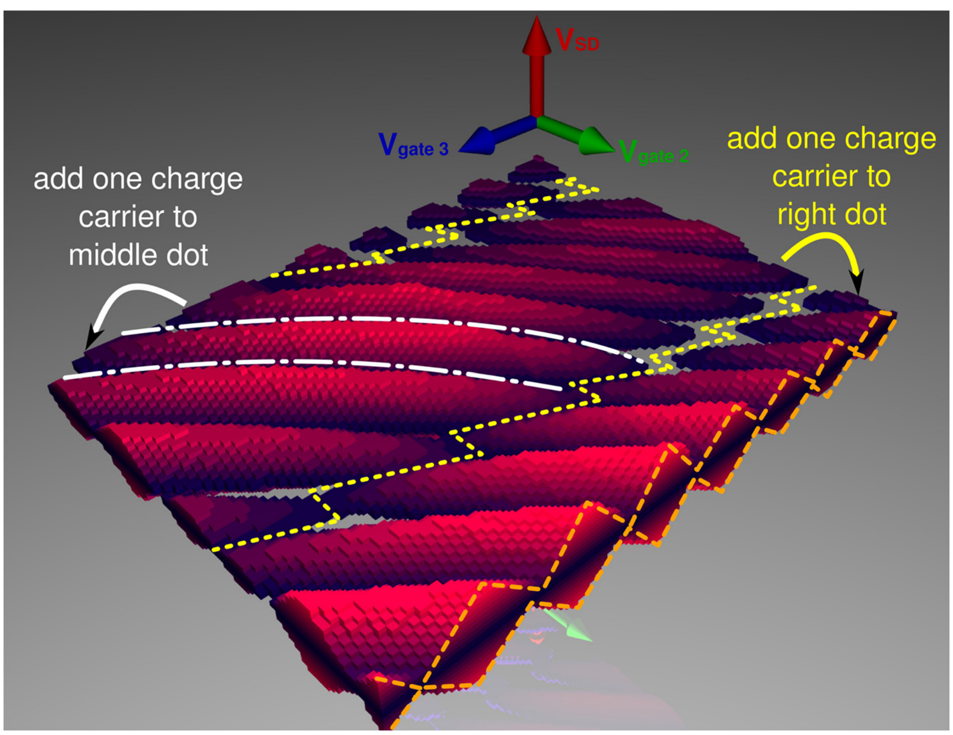

FIG. 21. "3D Coulomb diamonds": for each point in gate voltages 2 and 3, the current is measured as a function of applied bias voltage. If the current is below a certain limit, a box is plotted. The color of the boxes is given by the applied bias. Cuts at constant gate 2 or 3 result in Coulomb blockade diamond measurements similar to Fig. 18 (see orange dashed line). When the white line is crossed, an electron is loaded into the middle dot. When the yellow line is crossed, an electron is loaded into the right dot. It is clearly visible that the size of the Coulomb diamonds of the middle dot decreases when approaching the yellow line.

offer novel approaches for designing graphene quantum dot devices with possibly different characteristics.

1. CVD grown graphene islands

There are a number of different experiments where graphene quantum dots grown on an iridium surface were investigated by STM.[300–304] Besides mapping the topology of the graphene islands, the local density of states (LDOS) was probed as a function of position.[300–304] A modulation of the LDOS with position and dot geometry was found and interpreted as influences from quantum confinement[300,301,303,304] or as the observation of the wave function.[302] In a recent experiment, the graphene was intercalated by oxygen in order to exclude the influence of surface states of the iridium.[304] Interestingly, one experiment also showed that the modulation of the LDOS did not depend on the type of the edge.[301]

2. Chemically derived quantum dots

In another set of experiments, chemically produced and often functionalized graphene quantum dots were investigated. Reference 305 provides an overview over different fabrication techniques. A number of possible applications for graphene quantum dots were suggested such as photovoltaics,[306–308] light emitting diodes,[305,309–312] bioimaging,[309,313,314] sensors,[315] optoelectronics,[306,309,310,314] supercapacitors,[311] and fuel cells.[309] Notably, these quantum dots were found to be photoluminescent.[306,310,313,314] Singlet-triplet lifetimes of such chemically derived graphene quantum dots were measured optically[316] and found to be in the microsecond range. In a recent experiment, individual dots were probed and it was found that the optical spectrum did not depend on the dot size.[312] Also, electrical measurements of "piles" of such quantum dots were carried out.[317]

3. Strain-defined quantum dots

Along a different route was the experiment by Klimov *et al*.[318] where a graphene membrane was deformed by an STM tip and a quantum dot was formed due to the induced strain.

X. SUMMARY

In experiments, nanoribbons typically do not show quantized conductance as expected from theory for perfect nanoribbons. There are many possible imperfections that can alter transport properties. These imperfections can be roughly grouped into three categories: disorder from the environment, disorder from the graphene, and disorder from the edges. Effects such as charge traps in the oxide, substrate phonons, substrate roughness, or adsorbed molecules on top of the graphene fall into the first category. The second category includes effects such as lattice defects of the graphene or ripples. The third category covers edges that do not follow the principal crystal directions, reconstructed edges, and molecules bound to the edges. The steady improvement of device quality for micron sized graphene devices showed that the first two categories can be successfully addressed as in those devices edges only play a minor role.

Employing the same improvements in fabrication technology for reactive ion etched graphene nanodevices as for the micron sized graphene devices does, however, not result in a significant change of transport properties. This implies that imperfect and disordered edges are currently the major cause for the observed electronic transport properties of those graphene nanodevices. As transport properties for a wide range of devices are similar, those findings are likely also valid for many other fabrication approaches.

Electronic transport through graphene nanostructures is typically characterized by a reduced conductivity and a region of strongly suppressed conductance around the charge neutrality point. Although the presence of an energy gap due to quantum confinement can currently not be fully excluded, most experimental evidence points to another mechanism that is responsible for blocking current through nanodevices: charge localization resulting in Coulomb blockade. Many experiments performed on devices fabricated with different processes and methods have observed Coulomb blockade diamonds in graphene nanoribbons. It is therefore very likely that different kinds of edge disorder were present in the different devices. This indicates that the exact type of edge disorder is either unimportant or that due to some special energetic configuration all processes resulted in similar edges. The second possibility is rather unlikely as experiments probing edges with atomic resolution (mostly STM and TEM) showed different kinds of edge morphologies. Further, theory predicts that various different atomic configurations at the edges have similar energies such that it is unlikely that one of them always prevails.

So far, no clear difference in transport properties was found for ribbons fabricated out of single layer and bilayer graphene. This can again be interpreted as a sign that the details of the band structure of graphene are currently not probed in nanodevices as edge disorder is too strong.

Multiple mechanisms were suggested to be responsible for the localization of electrons inside graphene nanoribbons. Recent experiments have indicated that at least some localized states follow the edge of the device and extend out of the constriction along the edge of the graphene leads. These findings suggest that models relying on an energy gap due to quantum confinement are not capturing the whole picture as such an energy gap is unlikely to exist in the wide graphene leads adjacent to the ribbon. Numerical simulations of graphene stripes with disordered edges also managed to predict charge localization along the edges. From a theoretical point of view, the exact mechanism is, however, not fully understood: as the length on which charge is localized is about two orders of magnitude longer than the typical length on which edges are disordered, it is unlikely that electrons are localized at a single defect site. It is further unclear if the observed localization is related to the edge states predicted for perfect zig-zag ribbons. As the general crystallographic orientation of devices does, however, not seem to play an important role in experiments, this is unlikely. As a hand-waving argument, graphene edges are similar to the surfaces of three-dimensional crystals and it is therefore not surprising to find surface states due to the breaking of the crystal symmetry.

Most graphene nanodevices—ribbons or island shaped quantum dot geometries—showed multiple sites of localized charge that were capacitively and tunneling coupled to each other. Due to strong coupling of different sites in series, it is, however, still possible to observe well-behaving non-overlapping Coulomb diamonds. This was explained by higher order cotunneling processes where the outer dots mimic the role of tunneling barriers by allowing higher order cotunneling over virtual states. It is therefore important to have a sufficient number of external gates in a useful geometry to detect multiple sites of localized charge via their different capacitive coupling to different gates.

This presence of multiple sites of localized charges in series can explain why certain single dot physics such as the Kondo effect and double dot physics such as spin blockade are hard to observe in graphene nanodevices.

The transport properties of graphene nanodevices in ribbon and in island geometry are very similar. There is, however, a tendency that devices in island geometry show more regular and less overlapping Coulomb blockade diamonds.

It was further shown that interference effects in the graphene leads adjacent to the nanostructure can result in lines being roughly parallel to the Coulomb diamond edges. Care has therefore to be taken when attributing lines parallel to diamond edges to electronic excited states. It is further worth noting that many devices are typically in a multi-level transport regime where electronic excited states are so closely spaced that they cannot be resolved unless the coupling strength to the leads is sufficiently different.

There are, however, a number of exceptions where experiments showed qualitatively different properties. Examples are the unzipped carbon nanotubes from Ref. 46 that show signatures of Kondo effect or Ref. 56 showing quantized conductance in a current annealed suspended ribbon. Alternative approaches completely avoiding edges by electrostatically defining structures in bilayer graphene[61,234] or resulting in atomically perfect edges[151,222–226] exist. Finally, novel devices grown on step edges of SiC show promising properties as well.[228]

XI. OUTLOOK

Neither the exact mechanism for charge localization nor the exact spatial extent of localized wave functions is currently known in detail. It would therefore be interesting to combine imaging techniques like STM with low-temperature transport experiments. Such data would further allow to directly compare theoretical and numerical models with reality. First steps in this direction were performed by Qi *et al.*[145] where a TEM was used to image and manipulate graphene nanodevices while transport was recorded at room temperature.

Additional information on number, position, and movement of localized charge sites in graphene nanoribbons could be obtained by fabricating devices with multiple gates. Such an experiment might help to resolve the question whether a "quantum dot" picture is applicable, where electrons are loaded into the same site of localized charge repeatedly. The alternative picture would suggest that at different energies wave functions get localized at different positions.

There was much progress already in fabricating nanodevices with better control over the edges: bottom-up self-aligned nanoribbons from molecules, double-gated bilayer devices, and possibly also graphene ribbons on SiC step edges. Further work is, however, needed to fabricate nanodevices of arbitrary geometry in a reproducible way. A promising approach would be to functionalize edges of reactive ion etched structures.

Finally, there is a large number of other two-dimensional materials available: there are about 40 transition metal dichalcogenides[319] and a large number of further layered materials.[320–323] A combination of different materials together with nanostructures could yield in devices with superior properties. It would, for example, be possible to fabricate graphene quantum dots in a way where electrons need to tunnel through an atomic layer of an insulator into a graphene island with perfect edges grown by CVD and out again. This would possibly enable to measure well controlled single quantum dots in graphene and mark a significant step towards graphene spintronics.

ACKNOWLEDGMENTS

Financial support by the National Center of Competence in Research on "Quantum Science and Technology"(NCCR QSIT) funded by the Swiss National Science Foundation, by the Marie Curie ITNs S^3NANO, and by the QNET is gratefully acknowledged.

APPENDIX A: BAND GAP

Assuming a perfect, periodic, and infinite crystal, the choice of atoms and lattice will result in a band structure: electrons are allowed to exist only at certain energies for certain k-vectors (so-called "bands").[324] Energy ranges in the band structure where no electronic states are allowed to exist are called band gaps (see Fig. 22(b)).[324] If the Fermi energy lies within such a band gap and the size of the band gap is moderate, the system is considered as semiconductor.[324]

As in reality, crystals are never perfect and infinite; the general assumption for the above model to be valid is that the crystal is large and that the amount of perturbations is small.

The easiest way to experimentally measure the band gap at small k-vector is to perform an optical absorption measurement: if the energy of the light is smaller than the band gap of a semiconductor, light will not be absorbed.[324] Alternatively, optical emission experiments can be used where light with an energy higher than the band gap is shone on the crystal and the photons emitted by the semiconductor are investigated.[325]

Band gaps can also be measured with ARPES[326] or STM/STS,[327] but experiments are typically challenging.

If the band gap is sufficiently small, electronical measurements can also help to obtain information about its size. By increasing the temperature, electrons can be excited into the conduction band and thereby contribute to conduction.[328] The resulting scaling of the conductance (for undoped

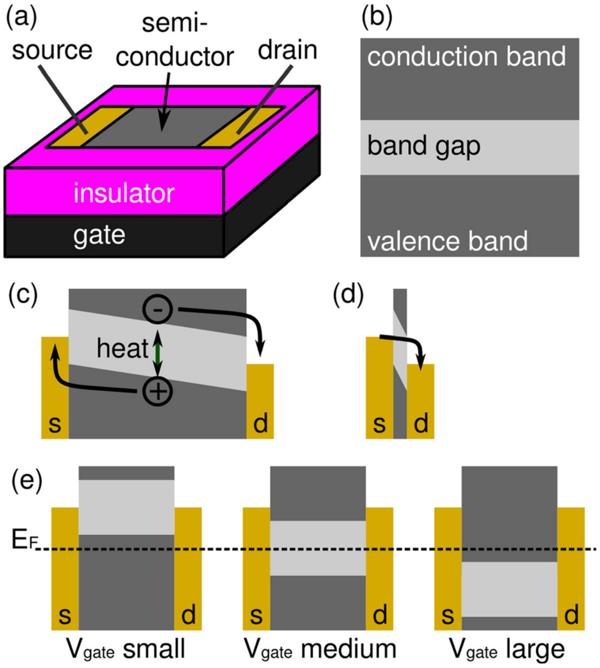

FIG. 22. (a) Typical device geometry for measurements. (b) Simplified band diagram of a semiconductor. (c) Increasing the temperature can provide energy to excite electron-hole pairs. By applying a bias between source and drain, these electron-hole pairs can be collected and current can flow. Current will generally depend on the device length. The temperature dependence of the current should, however, not depend on the device length, unless (d) the semiconductor region is so short that tunneling can occur. (e) If the gate voltage is chosen such that the Fermi energy lies in the band gap, conduction is suppressed. If the Fermi energy lies in the conduction or the valence band, current can flow.

semiconductors) will be proportional to the amount of excited charge carriers ($\propto \exp(-E/2k_BT)$).[328] This is schematically depicted in Fig. 22(c). As other effects as, for example, a change in mobility with temperature and phonons play a role[329] and as other physical effects have similar scaling (e.g., Refs. 166 and 203), this method is not especially reliable to extract a band gap.

Alternatively, a metal gate can be used to tune the Fermi energy from below the gap to above the gap. By converting the applied gate voltage difference into an energy, the gap can be calculated. Care has to be taken when converting gate voltages into energy, with the employed capacitor model and with quantum capacitance effects arising due to small densities. The process is depicted in Fig. 22(e).

As the band gap is a material property, it should in a first approximation not depend on the details of the device geometry. It is further worth noting that for various technological applications the presence of a band gap is necessary.

APPENDIX B: GLOSSARY

AFM: atomic force microscopy, similar to SFM
ARPES: angle resolved photon emission spectroscopy
BGG: back-gate gap – region of suppressed conductance in back gate voltage
CVD: chemical vapor deposition, graphene grown typically on metal foils from organic precursors
EBL: electron beam lithography
Expanded graphite: chemically exfoliated graphite
hBN: hexagonal boron nitride
HOPG: highly ordered pyrolithic graphite, similar to Kish graphite
Kish graphite: side product of steel fabrication
LDOS: local density of states
Natural graphite: graphite flakes obtained from mines, usually cleaned
RIE: reactive ion etching
SDG: source-drain gap – region of suppressed conductance in source-drain voltage
SEM: scanning electron microscopy
SET: single electron transistor
SFM: scanning force microscopy
SiC: crystalline silicon carbide
STM: scanning tunneling microscopy
STS: scanning tunneling spectroscopy
TEM: transmission electron microscopy
QPC: quantum point contact

[1]K. S. Novoselov, A. K. Geim, S. V. Morozov, D. Jiang, Y. Zhang, S. V. Dubonos, I. V. Grigorieva, and A. A. Firsov, "Electric field effect in atomically thin carbon films," Science **306**, 666–669 (2004).
[2]H. P. Boehm, A. Clauss, G. O. Fischer, and U. Hofmann, "Das Adsorptionsverhalten sehr dünner Kohlenstoff Folien," Z. Anorg. Allg. Chem. **316**, 119–127 (1962).
[3]A. J. van Bommel, J. E. Crombeen, and A. van Tooren, "LEED and Auger electron observation of the SiC(0001) surface," Surf. Sci. **48**, 463–472 (1975).
[4]T. J. Booth, P. Blake, R. R. Nair, D. Jiang, E. W. Hill, U. Bangert, A. Bleloch, M. Gass, K. S. Novoselov, M. I. Katsnelson, and A. K. Geim, "Macroscopic graphene membranes and their extraordinary stiffness," Nano Lett. **8**, 2442–2446 (2008).
[5]C. Lee, X. Wei, J. W. Kysar, and J. Hone, "Measurement of the elastic properties and intrinsic strength of monolayer graphene," Science **321**, 385 (2008).
[6]F. Schedin, A. K. Geim, S. V. Morozov, E. W. Hill, P. Blake, M. I. Katsnelson, and K. S. Novoselov, "Detection of individual gas molecules adsorbed on graphene," Nat. Mater. **6**, 652–655 (2007).
[7]R. R. Nair, P. Blake, A. N. Grigorenko, K. S. Novoselov, T. J. Booth, T. Stauber, N. M. R. Peres, and A. K. Geim, "Fine structure constant defines visual transparency of graphene," Science **320**, 1308 (2008).
[8]A. A. Balandin, S. Ghosh, W. Bao, I. Calizo, D. Teweldebrhan, F. Miao, and C. N. Lau, "Superior thermal conductivity of single-layer graphene," Nano Lett. **8**, 902–907 (2008).
[9]A. K. Geim, "Graphene: Status and prospects," Science **324**, 1530–1534 (2009).
[10]P. R. Wallace, "The band theory of graphite," Phys. Rev. **71**, 622–634 (1947).
[11]A. H. C. Neto, F. Guinea, N. M. R. Peres, K. S. Novoselov, and A. K. Geim, "The electronic properties of graphene," Rev. Mod. Phys. **81**, 109–162 (2009).
[12]S. D. Sarma, S. Adam, E. H. Hwang, and E. Rossi, "Electronic transport in two-dimensional graphene," Rev. Mod. Phys. **83**, 407–470 (2011).
[13]P. Kim, "Graphene and relativistic quantum physics," Semin. Poincare **18**, 1–21 (2014).
[14]M. I. Katsnelson, K. S. Novoselov, and A. K. Geim, "Chiral tunneling and the Klein paradox in graphene," Nat. Phys. **2**, 620–625 (2006).
[15]A. F. Young and P. Kim, "Quantum interference and Klein tunneling in graphene heterojunctions," Nat. Phys. **5**, 222–226 (2009).
[16]A. S. Mayorov, R. V. Gorbachev, S. V. Morozov, L. Britnell, R. Jalil, L. A. Ponomarenko, P. Blake, K. S. Novoselov, K. Watanabe, T. Taniguchi, and A. K. Geim, "Micrometer-scale ballistic transport in encapsulated graphene at room temperature," Nano Lett. **11**, 2396–2399 (2011).
[17]F. Schwierz, "Graphene transistors," Nat. Nanotechnol. **5**, 487–496 (2010).
[18]Y. Wu, Y.-M. Lin, A. A. Bol, K. A. Jenkins, F. Xia, D. B. Farmer, Y. Zhu, and P. Avouris, "High-frequency, scaled graphene transistors on diamond-like carbon," Nature **472**, 74–78 (2011).

[19]D. C. Elias, R. R. Nair, T. M. G. Mohiuddin, S. V. Morozov, P. Blake, M. P. Halsall, A. C. Ferrari, D. W. Boukhvalov, M. I. Katsnelson, A. K. Geim, and K. S. Novoselov, "Control of graphene's properties by reversible hydrogenation: Evidence for graphane," Science **323**, 610–613 (2009).
[20]J. T. Robinson, J. S. Burgess, C. E. Junkermeier, S. C. Badescu, T. L. Reinecke, F. K. Perkins, M. K. Zalalutdniov, J. W. Baldwin, J. C. Culbertson, P. E. Sheehan, and E. S. Snow, "Properties of fluorinated graphene films," Nano Lett. **10**, 3001–3005 (2010).
[21]E. V. Castro, K. S. Novoselov, S. V. Morozov, N. M. R. Peres, J. M. B. Lopes dos Santos, J. Nilsson, F. Guinea, A. K. Geim, and A. H. Castro Neto, "Biased bilayer graphene: Semiconductor with a gap tunable by the electric field effect," Phys. Rev. Lett. **99**, 216802 (2007).
[22]H. Yang, J. Heo, S. Park, H. J. Song, D. H. Seo, K.-E. Byun, P. Kim, I. Yoo, H.-J. Chung, and K. Kim, "Graphene barristor, a triode device with a gate-controlled Schottky barrier," Science **336**, 1140–1143 (2012).
[23]T. Georgiou, R. Jalil, B. D. Belle, L. Britnell, R. V. Gorbachev, S. V. Morozov, Y.-J. Kim, A. Gholinia, S. J. Haigh, O. Makarovsky, L. Eaves, L. A. Ponomarenko, A. K. Geim, K. S. Novoselov, and A. Mishchenko, "Vertical field-effect transistor based on graphene-WS2 heterostructures for flexible and transparent electronics," Nat. Nanotechnol. **8**, 100–103 (2013).
[24]K. Nakada, M. Fujita, G. Dresselhaus, and M. S. Dresselhaus, "Edge state in graphene ribbons: Nanometer size effect and edge shape dependence," Phys. Rev. B **54**, 17954–17961 (1996).
[25]B. Trauzettel, D. V. Bulaev, D. Losss, and G. Burkard, "Spin qubits in graphene quantum dots," Nat. Phys. **3**, 192–196 (2007).
[26]P. Recher and B. Trauzettel, "Quantum dots and spin qubits in graphene," Nanotechnology **21**, 302001 (2010).
[27]M. Fuchs, J. Schliemann, and B. Trauzettel, "Ultralong spin decoherence times in graphene quantum dots with a small number of nuclear spins," Phys. Rev. B **88**, 245441 (2013).
[28]H. Min, J. E. Hill, N. A. Sinitsyn, B. R. Sahu, L. Kleinman, and A. H. MacDonald, "Intrinsic and Rashba spin-orbit interactions in graphene sheets," Phys. Rev. B **74**, 165310 (2006).
[29]K. Ono and S. Tarucha, "Nuclear-spin-induced oscillatory current in spin-blockaded quantum dots," Phys. Rev. Lett. **92**, 256803 (2004).
[30]T. Meunier, I. T. Vink, L. H. Willems van Beveren, K.-J. Tielrooij, R. Hanson, F. H. L. Koppens, H. P. Tranitz, W. Wegscheider, L. P. Kouwenhoven, and L. M. K. Vandersypen, "Experimental signature of phonon-mediated spin relaxation in a two-electron quantum dot," Phys. Rev. Lett. **98**, 126601 (2007).
[31]D. Kochan, M. Gmitra, and J. Fabian, "Spin relaxation mechanism in graphene: Resonant scattering by magnetic impurities," Phys. Rev. Lett. **112**, 116602 (2014).
[32]S. Russo, J. B. Oostinga, D. Wehenkel, H. B. Heersche, S. S. Sobhani, L. M. K. Vandersypen, and A. F. Morpurgo, "Observation of Aharonov-Bohm conductance oscillations in a graphene ring," Phys. Rev. B **77**, 085413 (2008).
[33]L. Weng, L. Zhang, Y. P. Chen, and L. P. Rokhinson, "Atomic force microscope local oxidation nanolithography of graphene," Appl. Phys. Lett. **93**, 093107 (2008).
[34]M. Huefner, F. Molitor, A. Jacobsen, A. Pioda, C. Stampfer, K. Ensslin, and T. Ihn, "Investigation of the Aharonov–Bohm effect in a gated graphene ring," Phys. Status Solidi B **246**, 2756–2759 (2009).
[35]J. S. Yoo, Y. W. Park, V. Skákalová, and S. Roth, "Shubnikov–de Haas and Aharonov Bohm effects in a graphene nanoring structure," Appl. Phys. Lett. **96**, 143112 (2010).
[36]M. Huefner, F. Molitor, A. Jacobsen, A. Pioda, C. Stampfer, K. Ensslin, and T. Ihn, "The Aharonov–Bohm effect in a side-gated graphene ring," New J. Phys. **12**, 043054 (2010).
[37]D. Smirnov, H. Schmidt, and R. J. Haug, "Aharonov-Bohm effect in an electron-hole graphene ring system," Appl. Phys. Lett. **100**, 203114 (2012).
[38]S. Lakshmi, S. Roche, and G. Cuniberti, "Spin-valve effect in zigzag graphene nanoribbons by defect engineering," Phys. Rev. B **80**, 193404 (2009).
[39]G. Autes and O. V. Yazyev, "Engineering quantum spin Hall effect in graphene nanoribbons via edge functionalization," Phys. Rev. B **87**, 241404 (2013).
[40]D. Bischoff, A. Varlet, P. Simonet, T. Ihn, and K. Ensslin, "Electronic triple-dot transport through a bilayer graphene island with ultrasmall constrictions," New J. Phys. **15**, 083029 (2013).
[41]D. Goldhaber-Gordon, H. Shtrikman, D. Mahalu, D. Abusch-Magder, U. Meirav, and M. A. Kastner, "Kondo effect in a single-electron transistor," Nature **391**, 156–159 (1998).
[42]S. M. Cronenwett, T. H. Oosterkamp, and L. P. Kouwenhoven, "A tunable Kondo effect in quantum dots," Science **281**, 540–544 (1998).
[43]S. Tarucha, D. G. Austing, T. Honda, R. J. van der Hage, and L. P. Kouwenhoven, "Shell filling and spin effects in a few electron quantum dot," Phys. Rev. Lett. **77**, 3613–3616 (1996).
[44]D. H. Cobden, M. Bockrath, P. L. McEuen, A. G. Rinzler, and R. E. Smalley, "Spin splitting and even-odd effects in carbon nanotubes," Phys. Rev. Lett. **81**, 681–684 (1998).
[45]A. Jacobsen, P. Simonet, K. Ensslin, and T. Ihn, "Finite-bias spectroscopy of a three-terminal graphene quantum dot in the multilevel regime," Phys. Rev. B **89**, 165413 (2014).
[46]X. Wang, Y. Ouyang, L. Jiao, H. Wang, L. Xie, J. Wu, J. Guo, and H. Dai, "Graphene nanoribbons with smooth edges behave as quantum wires," Nat. Nanotechnol. **6**, 563–567 (2011).
[47]J. Güttinger, F. Molitor, C. Stampfer, S. Schnez, A. Jacobsen, S. Dröscher, T. Ihn, and K. Ensslin, "Transport through graphene quantum dots," Rep. Prog. Phys. **75**, 126502 (2012).
[48]A. K. Geim and K. S. Novoselov, "The rise of graphene," Nat. Mater. **6**, 183–191 (2007).
[49]X. Du, I. Skachko, A. Barker, and E. Y. Andrei, "Approaching ballistic transport in suspended graphene," Nat. Nanotechnol. **3**, 491–495 (2008).
[50]J. Martin, N. Akerman, G. Ulbricht, T. Lohmann, J. H. Smet, K. von Klitzing, and A. Yacoby, "Observation of electron–hole puddles in graphene using a scanning single-electron transistor," Nat. Phys. **4**, 144–148 (2008).
[51]J. C. Meyer, A. K. Geim, M. I. Katsnelson, K. S. Novoselov, T. J. Booth, and S. Roth, "The structure of suspended graphene sheets," Nature **446**, 60–63 (2007).
[52]J. Moser, A. Barreiro, and A. Bachtold, "Current-induced cleaning of graphene," Appl. Phys. Lett. **91**, 163513 (2007).
[53]K. I. Bolotin, K. J. Sikes, Z. Jiang, M. Klima, G. Fudenberg, J. Hone, P. Kim, and H. L. Stormer, "Ultrahigh electron mobility in suspended graphene," Solid State Commun. **146**, 351–355 (2008).
[54]K. I. Bolotin, K. J. Sikes, J. Hone, H. L. Stormer, and P. Kim, "Temperature-dependent transport in suspended graphene," Phys. Rev. Lett. **101**, 096802 (2008).
[55]A. S. Mayorov, D. C. Elias, I. S. Mukhin, S. V. Morozov, L. A. Ponomarenko, K. S. Novoselov, A. K. Geim, and R. V. Gorbachev, "How close can one approach the Dirac point in graphene experimentally?," Nano Lett. **12**, 4629–4634 (2012).
[56]N. Tombros, A. Veligura, J. Junesch, M. H. D. Guimarães, I. J. Vera-Marun, H. T. Jonkman, and B. J. van Wees, "Quantized conductance of a suspended graphene nanoconstriction," Nat. Phys. **7**, 697–700 (2011).
[57]W. Bao, K. Myhro, Z. Zhao, Z. Chen, W. Jang, L. Jing, F. Miao, H. Zhang, C. Dames, and C. N. Lau, "*In situ* observation of electrostatic and thermal manipulation of suspended graphene membranes," Nano Lett. **12**, 5470–5474 (2012).
[58]D.-K. Ki and A. F. Morpurgo, "High-quality multiterminal suspended graphene devices," Nano Lett. **13**, 5165–5170 (2013).
[59]R. Maurand, P. Rickhaus, P. Makk, S. Hess, E. Tovari, C. Handschin, M. Weiss, and C. Schönenberger, "Fabrication of ballistic suspended graphene with local-gating," Carbon **79**, 486–492 (2014).
[60]R. T. Weitz, M. T. Allen, B. E. Feldman, J. Martin, and A. Yacoby, "Broken-symmetry states in doubly gated suspended bilayer graphene," Science **330**, 812–816 (2010).
[61]M. T. Allen, J. Martin, and A. Yacoby, "Gate-defined quantum confinement in suspended bilayer graphene," Nat. Commun. **3**, 934 (2012).
[62]D.-K. Ki and A. F. Morpurgo, "Crossover from Coulomb blockade to quantum Hall effect in suspended graphene nanoribbons," Phys. Rev. Lett. **108**, 266601 (2012).
[63]C. R. Dean, A. F. Young, I. Meric, C. Lee, L. Wang, S. Sorgenfrei, K. Watanabe, T. Taniguchi, P. Kim, K. L. Shepard, and J. Hone, "Boron nitride substrates for high-quality graphene electronics," Nat. Nanotechnol. **5**, 722–726 (2010).
[64]K. M. Burson, W. G. Cullen, S. Adam, C. R. Dean, K. Watanabe, T. Taniguchi, P. Kim, and M. S. Fuhrer, "Direct imaging of charged impurity density in common graphene substrates," Nano Lett. **13**, 3576–3580 (2013).
[65]S. Ryu, L. Liu, S. Berciaud, Y.-J. Yu, H. Liu, P. Kim, G. W. Flynn, and L. E. Brus, "Atmospheric oxygen binding and hole doping in deformed graphene on a SiO_2 substrate," Nano Lett. **10**, 4944–4951 (2010).
[66]R. Decker, Y. Wang, V. W. Brar, W. Regan, H.-Z. Tsai, Q. Wu, W. Gannett, A. Zettl, and M. F. Crommie, "Local electronic properties of

graphene on a BN substrate via scanning tunneling microscopy," Nano Lett. **11**, 2291–2295 (2011).

[67]J. Xue, J. Sanchez-Yamagishi, D. Bulmash, P. Jacquod, A. Deshpande, K. Watanabe, T. Taniguchi, P. Jarillo-Herrero, and B. J. LeRoy, "Scanning tunneling microscopy and spectroscopy of ultra-flat graphene on hexagonal boron nitride," Nat. Mater. **10**, 282–285 (2011).

[68]S. J. Haigh, A. Gholinia, R. Jalil, S. Romani, L. Britnell, D. C. Elias, K. S. Novoselov, L. A. Ponomarenko, A. K. Geim, and R. Gorbachev, "Cross-sectional imaging of individual layers and buried interfaces of graphene-based heterostructures and superlattices," Nat. Mater. **11**, 764–767 (2012).

[69]L. Wang, I. Meric, P. Y. Huang, Q. Gao, Y. Gao, H. Tran, T. Taniguchi, K. Watanabe, L. M. Campos, D. A. Muller, J. Guo, P. Kim, J. Hone, K. L. Shepard, and C. R. Dean, "One-dimensional electrical contact to a two-dimensional material," Science **342**, 614–617 (2013).

[70]P. Maher, L. Wang, Y. Gao, C. Forsythe, T. Taniguchi, K. Watanabe, D. Abanin, Z. Papic, P. Cadden-Zimansky, J. Hone, P. Kim, and C. R. Dean, "Tunable fractional quantum Hall phases in bilayer graphene," Science **345**, 61–64 (2014).

[71]P. J. Zomer, M. H. D. Guimaraes, J. C. Brant, N. Tombros, and B. J. van Wees, "Fast pick up technique for high quality heterostructures of bilayer graphene and hexagonal boron nitride," Appl. Phys. Lett. **105**, 013101 (2014).

[72]M. H. D. Guimaraes, P. J. Zomer, J. Ingla-Aynes, J. C. Brant, N. Tombros, and B. J. van Wees, "Controlling spin relaxation in hexagonal BN-encapsulated graphene with a transverse electric field," Phys. Rev. Lett. **113**, 086602 (2014).

[73]Z. Li, Y. Wang, A. Kozbial, G. Shenoy, F. Zhou, R. McGinley, P. Ireland, B. Morganstein, A. Kunkel, S. P. Surwade, L. Li, and H. Liu, "Effect of airborne contaminants on the wettability of supported graphene and graphite," Nat. Mater. **12**, 925–931 (2013).

[74]X. Wu, Y. Hu, M. Ruan, N. K. Madiomanana, J. Hankinson, M. Sprinkle, C. Berger, and W. A. de Heer, "Half integer quantum Hall effect in high mobility single layer epitaxial graphene," Appl. Phys. Lett. **95**, 223108 (2009).

[75]S. Tanabe, Y. Sekine, H. Kageshima, M. Nagase, and H. Hibino, "Carrier transport mechanism in graphene on SiC(0001)," Phys. Rev. B **84**, 115458 (2011).

[76]S. Kopylov, A. Tzalenchuk, S. Kubatkin, and V. I. Fal'ko, "Charge transfer between epitaxial graphene and silicon carbide," Appl. Phys. Lett. **97**, 112109 (2010).

[77]T. J. B. M. Janssen, A. Tzalenchuk, R. Yakimova, S. Kubatkin, S. Lara-Avila, S. Kopylov, and V. I. Fal'ko, "Anomalously strong pinning of the filling factor $\nu=2$ in epitaxial graphene," Phys. Rev. B **83**, 233402 (2011).

[78]J. A. Alexander-Webber, A. M. R. Baker, T. J. B. M. Janssen, A. Tzalenchuck, S. Lara-Avila, S. Kubatkin, R. Yakimova, B. A. Piot, D. K. Maude, and R. J. Nicholas, "Phase space for the breakdown of the quantum Hall effect in epitaxial graphene," Phys. Rev. Lett. **111**, 096601 (2013).

[79]T. Ando, "The electronic properties of graphene and carbon nanotubes," NPG Asia Mater. **1**, 17–21 (2009).

[80]M. Acik and Y. J. Chabal, "Nature of graphene edges: A review," Jpn. J. Appl. Phys., Part 1 **50**, 070101 (2011).

[81]M. Fujita, K. Wakabayashi, K. Nakada, and K. Kusakabe, "Peculiar localized state at zigzag graphite edge," J. Phys. Soc. Jpn. **65**, 1920–1923 (1996).

[82]D. A. Areshkin, D. Gunlycke, and C. T. White, "Ballistic transport in graphene nanostrips in the presence of disorder: Importance of edge effects," Nano Lett. **7**, 204–210 (2007).

[83]V. Barone, O. Hod, and G. Scuseria, "Electronic structure and stability of semiconducting graphene nanoribbons," Nano Lett. **6**, 2748–2754 (2006).

[84]Y.-W. Son, M. L. Cohen, and S. G. Louie, "Energy gaps in graphene nanoribbons," Phys. Rev. Lett. **97**, 216803 (2006).

[85]P. Koskinen, S. Malola, and H. Häkkinen, "Self-passivating edge reconstructions of graphene," Phys. Rev. Lett. **101**, 115502 (2008).

[86]B. Huang, M. Liu, N. Su, J. Wu, W. Duan, B.-L. Gu, and F. Liu, "Quantum manifestations of graphene edge stress and edge instability: A first-principles study," Phys. Rev. Lett. **102**, 166404 (2009).

[87]Q. Lu and R. Huang, "Excess energy and deformation along free edges of graphene nanoribbons," Phys. Rev. B **81**, 155410 (2010).

[88]T. Wassmann, A. P. Seitsonen, A. M. Saitta, M. Lazzeri, and F. Mauri, "Structure, stability, edge states, and aromaticity of graphene ribbons," Phys. Rev. Lett. **101**, 096402 (2008).

[89]S. M.-M. Dubois, A. Lopez-Bezanilla, A. Cresti, F. Triozon, B. Biel, J.-C. Charlier, and S. Roche, "Quantum transport in graphene nanoribbons: Effects of edge reconstruction and chemical reactivity," ACS Nano **4**, 1971–1976 (2010).

[90]P. Hawkins, M. Begliarbekov, M. Zivkovic, S. Strauf, and C. P. Search, "Quantum transport in graphene nanoribbons with realistic edges," J. Phys. Chem. C **116**, 18382–18387 (2012).

[91]S. Ihnatsenka and G. Kirczenow, "Effect of edge reconstruction and electron-electron interactions on quantum transport in graphene nanoribbons," Phys. Rev. B **88**, 125430 (2013).

[92]P. Wagner, V. V. Ivanovskaya, M. Melle-Franco, B. Humbert, J.-J. Adjizian, P. R. Briddon, and C. P. Ewels, "Stable hydrogenated graphene edge types: Normal and reconstructed Klein edges," Phys. Rev. B **88**, 094106 (2013).

[93]R. Ramprasad, P. von Allmen, and L. R. C. Fonseca, "Contributions to the work function: A density-functional study of adsorbates at graphene ribbon edges," Phys. Rev. B **60**, 6023 (1999).

[94]N. Gorjizadeh and Y. Kawazoe, "Chemical functionalization of graphene nanoribbons," J. Nanomater. **2010**, 513501.

[95]P. Wagner, C. P. Ewels, J.-J. Adjizian, L. Magaud, P. Pochet, S. Roche, A. Lopez-Bezanilla, V. V. Ivanovskaya, A. Yaya, M. Rayson, P. Briddon, and B. Humbert, "Band gap engineering via edge-functionalization of graphene nanoribbons," Phys. Chem. C **117**, 26790–26796 (2013).

[96]J. Dauber, B. Terres, C. Volk, S. Trellenkamp, and C. Stampfer, "Reducing disorder in graphene nanoribbons by chemical edge modification," Appl. Phys. Lett. **104**, 083105 (2014).

[97]X. Wang, S. M. Tabakman, and H. Dai, "Atomic layer deposition of metal oxides on pristine and functionalized graphene," J. Am. Chem. Soc. **130**, 8152–8153 (2008).

[98]T. Kato, L. Jiao, X. Wang, H. Wang, X. Li, L. Zhang, R. Hatakeyama, and H. Dai, "Room-temperature edge functionalization and doping of graphene by mild plasma," Small **7**, 574–577 (2011).

[99]R. Sekiya, Y. Uemura, H. Murakami, and T. Haino, "White-light-emitting edge-functionalized graphene quantum dots," Angew. Chem. **126**, 5725–5729 (2014).

[100]D. Gunlycke, D. A. Areshkin, and C. T. White, "Semiconducting graphene nanostrips with edge disorder," Appl. Phys. Lett. **90**, 142104 (2007).

[101]D. Basu, M. J. Gilbert, L. F. Register, and S. K. Banerjee, "Effect of edge roughness on electronic transport in graphene nanoribbon channel metal-oxide-semiconductor field-effect transistors," Appl. Phys. Lett. **92**, 042114 (2008).

[102]T. C. Li and S.-P. Lu, "Quantum conductance of graphene nanoribbons with edge defects," Phys. Rev. B **77**, 085408 (2008).

[103]M. Evaldsson, I. V. Zozoulenko, H. Xu, and T. Heinzel, "Edge-disorder-induced Anderson localization and conduction gap in graphene nanoribbons," Phys. Rev. B **78**, 161407(R) (2008).

[104]I. Martin and Ya. M. Blanter, "Transport in disordered graphene nanoribbons," Phys. Rev. B **79**, 235132 (2009).

[105]A. Cresti and S. Roche, "Range and correlation effects in edge disordered graphene nanoribbons," New J. Phys. **11**, 095004 (2009).

[106]E. R. Mucciolo, A. H. C. Neto, and C. H. Lewenkopf, "Conductance quantization and transport gaps in disordered graphene nanoribbons," Phys. Rev. B **79**, 075407 (2009).

[107]D. Querlioz, Y. Apertet, A. Valentin, K. Huet, A. Bournel, S. Galdin-Retailleau, and P. Dollfus, "Suppression of the orientation effects on bandgap in graphene nanoribbons in the presence of edge disorder," Appl. Phys. Lett. **92**, 042108 (2008).

[108]A. Pieper, G. Schubert, G. Wellein, and H. Fehske, "Effects of disorder and contacts on transport through graphene nanoribbons," Phys. Rev. B **88**, 195409 (2013).

[109]R. Reiter, U. Derra, S. Birner, B. Terres, F. Libisch, J. Burgdörfer, and C. Stampfer, "Negative quantum capacitance in graphene nanoribbons with lateral gates," Phys. Rev. B **89**, 115406 (2014).

[110]K. Wakabayashi and M. Sigrist, "Zero-conductance resonances due to flux states in nanographite ribbon junctions," Phys. Rev. Lett. **84**, 3390–3393 (2000).

[111]H. Xu, T. Heinzel, and I. V. Zozoulenko, "Edge disorder and localization regimes in bilayer graphene nanoribbons," Phys. Rev. B **80**, 045308 (2009).

[112]S. Ihnatsenka and G. Kirczenow, "Conductance quantization in graphene nanoconstrictions with mesoscopically smooth but atomically stepped boundaries," Phys. Rev. B **85**, 121407 (2012).

[113]F. Libisch, S. Rotter, and J. Burgdörfer, "Coherent transport through graphene nanoribbons in the presence of edge disorder," New J. Phys. **14**, 123006 (2012).

[114]I. Kleftogiannis, I. Amanatidis, and V. A. Gopar, "Conductance through disordered graphene nanoribbons: Standard and anomalous electron localization," Phys. Rev. B **88**, 205414 (2013).
[115]K. Wakabayashi, "Electronic transport properties of nanographite ribbon junctions," Phys. Rev. B **64**, 125428 (2001).
[116]F. Munoz-Rojas, D. Jacob, J. Fernández-Rossier, and J. J. Palacios, "Coherent transport in graphene nanoconstrictions," Phys. Rev. B **74**, 195417 (2006).
[117]A. Rycerz, J. Tworzydlo, and C. W. J. Beenakker, "Valley filter and valley valve in graphene," Nat. Phys. **3**, 172–175 (2007).
[118]P. Darancet, V. Olevano, and D. Mayou, "Coherent electronic transport through graphene constrictions: Subwavelength regime and optical analogy," Phys. Rev. Lett. **102**, 136803 (2009).
[119]J. Wurm, M. Wimmer, I. Adagideli, K. Richter, and H. U. Baranger, "Interfaces within graphene nanoribbons," New J. Phys. **11**, 095022 (2009).
[120]L.-L. Jiang, L. Huang, R. Yang, and Y.-C. Lai, "Control of transmission in disordered graphene nanojunctions through stochastic resonance," Appl. Phys. Lett. **96**, 262114 (2010).
[121]F. Libisch, S. Rotter, and J. Burgdörfer, "Disorder scattering in graphene nanoribbons," Phys. Status Solidi B **248**, 2598–2603 (2011).
[122]H.-Y. Deng, K. Wakabayashi, and C.-H. Lam, "Formation mechanism of bound states in graphene point contacts," Phys. Rev. B **89**, 045423 (2014).
[123]F. Sols, F. Guinea, and A. H. C. Neto, "Coulomb blockade in graphene nanoribbons," Phys. Rev. Lett. **99**, 166803 (2007).
[124]C. Archambault and A. Rochefort, "States modulation in graphene nanoribbons through metal contacts," ACS Nano **7**, 5414–5420 (2013).
[125]M. Ijäs, M. Ervasti, A. Uppstu, P. Liljeroth, J. van der Lit, I. Swart, and A. Harju, "Electronic states in finite graphene nanoribbons: Effect of charging and defects," Phys. Rev. B **88**, 075429 (2013).
[126]A. A. Shylau, J. W. Klos, and I. V. Zozoulenko, "Capacitance of graphene nanoribbons," Phys. Rev. B **80**, 205402 (2009).
[127]Y. M. You, Z. H. Ni, T. Yu, and Z. X. Shen, "Edge chirality determination of graphene by Raman spectroscopy," Appl. Phys. Lett. **93**, 163112 (2008).
[128]C. Casiraghi, A. Hartschuh, H. Qian, S. Piscanec, C. Georgi, A. Fasoli, K. S. Novoselov, D. M. Basko, and A. C. Ferrari, "Raman spectroscopy of graphene edges," Nano Lett. **9**, 1433–1441 (2009).
[129]Y. N. Xu, D. Zhan, L. Liu, H. Suo, Z. H. Ni, T. T. Nguyen, C. Zhao, and Z. X. Shen, "Thermal dynamics of graphene edges investigated by polarized Raman spectroscopy," ACS Nano **5**, 147–152 (2011).
[130]B. Krauss, P. Nemes-Incze, V. Skakalova, L. P. Biro, K. v. Klitzing, and J. H. Smet, "Raman scattering at pure graphene zigzag edges," Nano Lett. **10**, 4544–4548 (2010).
[131]D. Bischoff, J. Güttinger, S. Dröscher, T. Ihn, K. Ensslin, and C. Stampfer, "Raman spectroscopy on etched graphene nanoribbons," J. Appl. Phys. **109**, 073710 (2011).
[132]S. Ryu, J. Maultzsch, M. Y. Han, P. Kim, and L. E. Brus, "Raman spectroscopy of lithographically patterned graphene nanoribbons," ACS Nano **5**, 4123–4130 (2011).
[133]L. Xie, H. Wang, C. Jin, X. Wang, L. Jiao, K. Suenaga, and H. Dai, "Graphene nanoribbons from unzipped carbon nanotubes: Atomic structures, Raman spectroscopy, and electrical properties," J. Am. Chem. Soc. **133**, 10394–10397 (2011).
[134]R. Yang, Z. Shi, L. Zhang, D. Shi, and G. Zhang, "Observation of Raman G-peak split for graphene nanoribbons with hydrogen-terminated zigzag edges," Nano Lett. **11**, 4083–4088 (2011).
[135]L. G. Cancado, M. A. Pimenta, B. R. A. Neves, M. S. S. Dantas, and A. Jorio, "Influence of the atomic structure on the Raman spectra of graphite edges," Phys. Rev. Lett. **93**, 247401 (2004).
[136]A. Chuvilin, J. C. Meyer, G. Algara-Siller, and U. Kaiser, "From graphene constrictions to single carbon chains," New J. Phys. **11**, 083019 (2009).
[137]C. Ö. Girit, J. C. Meyer, R. Erni, M. D. Rossell, C. Kisielowski, L. Yang, C.-H. Park, M. F. Crommie, M. L. Cohen, S. G. Louie, and A. Zettl, "Graphene at the edge: Stability and dynamics," Science **323**, 1705–1708 (2009).
[138]X. Jia, M. Hofmann, V. Meunier, B. G. Sumpter, J. Campos-Delgado, J. M. Romo-Herrera, H. Son, Y.-P. Hsieh, A. Reina, J. Kong, M. Terrones, and M. S. Dresselhaus, "Controlled formation of sharp zigzag and armchair edges in graphitic nanoribbons," Science **323**, 1701–1705 (2009).
[139]P. Koskinen, S. Malola, and H. Häkkinen, "Evidence for graphene edges beyond zigzag and armchair," Phys. Rev. B **80**, 073401 (2009).
[140]Z. Liu, K. Suenaga, P. J. F. Harris, and S. Iijima, "Open and closed edges of graphene layers," Phys. Rev. Lett. **102**, 015501 (2009).
[141]K. Suenaga and M. Koshino, "Atom-by-atom spectroscopy at graphene edge," Nature **468**, 1088–1090 (2010).
[142]R. Zan, Q. M. Ramasse, U. Bangert, and K. S. Novoselov, "Graphene reknits its holes," Nano Lett. **12**, 3936–3940 (2012).
[143]A. Sinitskii, A. A. Fursina, D. V. Kosynkin, A. L. Higginbotham, D. Natelson, and J. M. Tour, "Electronic transport in monolayer graphene nanoribbons produced by chemical unzipping of carbon nanotubes," Appl. Phys. Lett. **95**, 253108 (2009).
[144]L. Jiao, X. Wang, G. Diankov, H. Wang, and H. Dai, "Facile synthesis of high-quality graphene nanoribbons," Nat. Nanotechnol. **5**, 321–325 (2010).
[145]Z. J. Qi, J. A. Rodriguez-Manzo, A. R. Botello-Mendez, S. J. Hong, E. A. Stach, Y. W. Park, J.-C. Charlier, M. Drndic, and A. T. C. Johnson, "Correlating atomic structure and transport in suspended graphene nanoribbons," Nano Lett. **14**, 4238–4244 (2014).
[146]Y. Niimi, T. Matsui, H. Kambara, K. Tagami, M. Tsukada, and H. Fukuyama, "Scanning tunneling microscopy and spectroscopy of the electronic local density of states of graphite surfaces near monoatomic step edges," Phys. Rev. B **73**, 085421 (2006).
[147]K. A. Ritter and J. W. Lyding, "The influence of edge structure on the electronic properties of graphene quantum dots and nanoribbons," Nat. Mater. **8**, 235–242 (2009).
[148]R. Yang, L. Zhang, Y. Wang, Z. Shi, D. Shi, H. Gao, E. Wang, and G. Zhang, "An anisotropic etching effect in the graphene basal plane," Adv. Mater. **22**, 4014–4019 (2010).
[149]X. Zhang, O. V. Yazyev, J. Feng, L. Xie, C. Tao, Y.-C. Chen, L. Jiao, Z. Pedramrazi, A. Zettl, S. G. Louie, H. Dai, and M. F. Crommie, "Experimentally engineering the edge termination of graphene nanoribbons," ACS Nano **7**, 198–202 (2013).
[150]Y. Kobayashi, K. Fukui, T. Enoki, and K. Kusakabe, "Edge state on hydrogen-terminated graphite edges investigated by scanning tunneling microscopy," Phys. Rev. B **73**, 125415 (2006).
[151]J. Cai, P. Ruffieux, R. Jaafar, M. Bieri, T. Braun, S. Blankenburg, M. Muoth, A. P. Seitsonen, M. Saleh, X. Feng, K. Müllen, and R. Fasel, "Atomically precise bottom-up fabrication of graphene nanoribbons," Nature **466**, 470–473 (2010).
[152]C. Tao, L. Jiao, O. V. Yazyev, Y.-C. Chen, J. Feng, X. Zhang, R. B. Capaz, J. M. Tour, A. Zettl, S. G. Louie, H. Dai, and M. F. Crommie, "Spatially resolving edge states of chiral graphene nanoribbons," Nat. Phys. **7**, 616–620 (2011).
[153]M. Pan, E. C. Girao, X. Jia, S. Bhaviripudi, Q. Li, J. Kong, V. Meunier, and M. S. Dresselhaus, "Topographic and spectroscopic characterization of electronic edge states in CVD grown graphene nanoribbons," Nano Lett. **12**, 1928–1933 (2012).
[154]X. Jia, J. Campos-Delgado, E. E. Gracia-Espino, M. Hofmann, H. Muramatsu, Y. A. Kim, T. Hayashi, M. Endo, J. Kong, M. Terrones, and M. S. Dresselhaus, "Loop formation in graphitic nanoribbon edges using furnace heating or Joule heating," J. Vac. Sci. Technol., B **27**, 1996 (2009).
[155]W. J. Yu, S. H. Chae, D. Perello, S. Y. Lee, G. H. Han, M. Yun, and Y. H. Lee, "Synthesis of edge-closed graphene ribbons with enhanced conductivity," ACS Nano **4**, 5480–5486 (2010).
[156]Z. Chen, Y.-M. Lin, M. J. Rooks, and P. Avouris, "Graphene nano-ribbon electronics," Physica E **40**, 228–232 (2007).
[157]M. Y. Han, B. Özyilmaz, Y. Zhang, and P. Kim, "Energy band-gap engineering of graphene nanoribbons," Phys. Rev. Lett. **98**, 206805 (2007).
[158]B. Özyilmaz, P. Jarillo-Herrero, D. Efetov, and P. Kim, "Electronic transport in locally gated graphene nanoconstrictions," Appl. Phys. Lett. **91**, 192107 (2007).
[159]S. Adam, S. Cho, M. S. Fuhrer, and S. D. Sarma, "Density inhomogeneity driven percolation metal-insulator transition and dimensional crossover in graphene nanoribbons," Phys. Rev. Lett. **101**, 046404 (2008).
[160]X. Liu, J. B. Oostinga, A. F. Morpurgo, and L. M. K. Vandersypen, "Electrostatic confinement of electrons in graphene nanoribbons," Phys. Rev. B **80**, 121407 (2009).
[161]R. Murali, Y. Yang, K. Brenner, T. Beck, and J. D. Meindl, "Breakdown current density of graphene nanoribbons," Appl. Phys. Lett. **94**, 243114 (2009).
[162]K. Todd, H.-T. Chou, S. Amasha, and D. Goldhaber-Gordon, "Quantum dot behavior in graphene nanoconstrictions," Nano Lett. **9**, 416–421 (2009).
[163]J. Bai, X. Duan, and Y. Huang, "Rational fabrication of graphene nanoribbons using a nanowire etch mask," Nano Lett. **9**, 2083–2087 (2009).

[164]J. Bai, R. Cheng, F. Xiu, L. Liao, M. Wang, A. Shailos, K. L. Wang, Y. Huang, and X. Duan, "Very large magnetoresistance in graphene nanoribbons," Nat. Nanotechnol. **5**, 655–659 (2010).
[165]P. Gallagher, K. Todd, and D. Goldhaber-Gordon, "Disorder-induced gap behavior in graphene nanoribbons," Phys. Rev. B **81**, 115409 (2010).
[166]M. Y. Han, J. C. Brant, and P. Kim, "Electron transport in disordered graphene nanoribbons," Phys. Rev. Lett. **104**, 056801 (2010).
[167]Y. Yang and R. Murali, "Impact of size effect on graphene nanoribbon transport," IEEE Electron Device Lett. **31**, 237–239 (2010).
[168]C. Lian, K. Tahy, T. Fang, G. Li, H. G. Xing, and D. Jena, "Quantum transport in graphene nanoribbons patterned by metal masks," Appl. Phys. Lett. **96**, 103109 (2010).
[169]L. Liao, J. Bai, Y.-C. Lin, Y. Qu, Y. Huang, and X. Duan, "High-performance top-gated graphene-nanoribbon transistors using zirconium oxide nanowires as high-dielectric-constant gate dielectrics," Adv. Mater. **22**, 1941–1945 (2010).
[170]L. Liao, J. Bai, R. Cheng, Y.-C. Lin, S. Jiang, Y. Huang, and X. Duan, "Top-gated graphene nanoribbon transistors with ultrathin high-k dielectrics," Nano Lett. **10**, 1917–1921 (2010).
[171]A. D. Liao, J. Z. Wu, X. Wang, K. Tahy, D. Jena, H. Dai, and E. Pop, "Thermally limited current carrying ability of graphene nanoribbons," Phys. Rev. Lett. **106**, 256801 (2011).
[172]Y.-S. Shin, J. Y. Son, M.-H. Jo, Y.-H. Shin, and H. M. Jang, "High-mobility graphene nanoribbons prepared using polystyrene dip-pen nanolithography," J. Am. Chem. Soc. **133**, 5623–5625 (2011).
[173]R. Ribeiro, J.-M. Poumirol, A. Cresti, W. Escoffier, M. Goiran, J.-M. Broto, S. Roche, and B. Raquet, "Unveiling the magnetic structure of graphene nanoribbons," Phys. Rev. Lett. **107**, 086601 (2011).
[174]M. Wang, E. B. Song, S. Lee, J. Tang, M. Lang, C. Zeng, G. Xu, Y. Zhou, and K. L. Wang, "Quantum dot behavior in bilayer graphene nanoribbons," ACS Nano **5**, 8769–8773 (2011).
[175]Y.-J. Yu, M. Y. Han, S. Berciaud, A. B. Georgescu, T. F. Heinz, L. E. Brus, K. S. Kim, and P. Kim, "High-resolution spatial mapping of the temperature distribution of a Joule self-heated graphene nanoribbon," Appl. Phys. Lett. **99**, 183105 (2011).
[176]A. Behnam, A. S. Lyons, M.-H. Bae, E. K. Chow, S. Islam, C. M. Neumann, and E. Pop, "Transport in nanoribbon interconnects obtained from graphene grown by chemical vapor deposition," Nano Lett. **12**, 4424–4430 (2012).
[177]S. Nakaharai, T. Iijima, S. Ogawa, H. Miyazaki, S. Li, K. Tsukagoshi, S. Sato, and N. Yokoyama, "Gate-controlled P–I–N junction switching device with graphene nanoribbon," Appl. Phys. Express **5**, 015101 (2012).
[178]W. J. Yu and X. Duan, "Tunable transport gap in narrow bilayer graphene nanoribbons," Sci. Rep. **3**, 1248 (2013).
[179]M. J. Hollander, H. Madan, N. Shukla, D. A. Snyder, J. A. Robinson, and S. Datta, "Short-channel graphene nanoribbon transistors with enhanced symmetry between p- and n-branches," Appl. Phys. Express **7**, 055103 (2014).
[180]W. S. Hwang, P. Zhao, K. Tahy, L. O. Nyakiti, V. D. Wheeler, R. L. Myers-Ward, C. R. Eddy, Jr., D. K. Gaskill, J. A. Robinson, W. Haensch, H. Xing, A. Seabaugh, and D. Jena, "Graphene nanoribbon field-effect transistors on wafer-scale epitaxial graphene on SiC substrates," APL Mater. **3**, 011101 (2015).
[181]P. Simonet, D. Bischoff, A. Moser, T. Ihn, and K. Ensslin, "Graphene nanoribbons: Relevance of etching process," J. Appl. Phys. **117**, 184303 (2015).
[182]Y. M. Lin, V. Perebeinos, Z. Chen, and P. Avouris, "Electrical observation of subband formation in graphene nanoribbons," Phys. Rev. B **78**, 161409 (2008).
[183]Y.-M. Lin and P. Avouris, "Strong suppression of electrical noise in bilayer graphene nanodevices," Nano Lett. **8**, 2119–2125 (2008).
[184]A. Fasoli, A. Colli, A. Lombardo, and A. C. Ferrari, "Fabrication of graphene nanoribbons via nanowire lithography," Phys. Status Solidi B **246**, 2514–2517 (2009).
[185]X. Liang, Y.-S. Jung, S. Wu, A. Ismach, D. L. Olynick, S. Cabrini, and J. Bokor, "Formation of bandgap and subbands in graphene nanomeshes with sub-10 nm ribbon width fabricated via nanoimprint lithography," Nano Lett. **10**, 2454–2460 (2010).
[186]A. Candini, S. Klyatskaya, M. Ruben, W. Wernsdorfer, and M. Affronte, "Graphene spintronic devices with molecular nanomagnets," Nano Lett. **11**, 2634–2639 (2011).
[187]W. S. Hwang, K. Tahy, X. Li, H. Xing, A. C. Seabaugh, C. Y. Sung, and D. Jena, "Transport properties of graphene nanoribbon transistors on chemical-vapor-deposition grown wafer-scale graphene," Appl. Phys. Lett. **100**, 203107 (2012).
[188]W. S. Hwang, K. Tahy, L. O. Nyakiti, V. D. Wheeler, R. L. Myers-Ward, C. R. Eddy, Jr., D. K. Gaskill, H. Xing, A. Seabaugh, and D. Jena, "Fabrication of top-gated epitaxial graphene nanoribbon FETs using hydrogen-silsesquioxane," J. Vac. Sci. Technol., B **30**, 03D104 (2012).
[189]S. Minke, S. H. Jhang, J. Wurm, Y. Skourski, J. Wosnitza, C. Strunk, D. Weiss, K. Richter, and J. Eroms, "Magnetotransport through graphene nanoribbons at high magnetic fields," Phys. Rev. B **85**, 195432 (2012).
[190]S. Minke, J. Bundesmann, D. Weiss, and J. Eroms, "Phase coherent transport in graphene nanoribbons and graphene nanoribbon arrays," Phys. Rev. B **86**, 155403 (2012).
[191]X. Liang and S. Wi, "Transport characteristics of multichannel transistors made from densely aligned sub-10 nm half-pitch graphene nanoribbons," ACS Nano **6**, 9700–9710 (2012).
[192]V. Abramova, A. S. Slesarev, and J. M. Tour, "Meniscus-mask lithography for narrow graphene nanoribbons," ACS Nano **7**, 6894–6898 (2013).
[193]P. D. Nguyen, T. C. Nguyen, A. T. Huynh, and E. Skafidas, "High frequency characterization of graphene nanoribbon interconnects," Mater. Res. Express **1**, 035009 (2014).
[194]D.-H. Chae, B. Krauss, K. v. Klitzing, and J. H. Smet, "Hot phonons in an electrically biased graphene constriction," Nano Lett. **10**, 466–471 (2010).
[195]J. B. Oostinga, B. Sacépé, M. F. Craciun, and A. F. Morpurgo, "Magnetotransport through graphene nanoribbons," Phys. Rev. B **81**, 193408 (2010).
[196]R. Danneau, F. Wu, M. Y. Tomi, J. B. Oostinga, A. F. Morpurgo, and P. J. Hakonen, "Shot noise suppression and hopping conduction in graphene nanoribbons," Phys. Rev. B **82**, 161405 (2010).
[197]F. Duerr, J. B. Oostinga, C. Gould, and L. W. Molenkamp, "Edge state transport through disordered graphene nanoribbons in the quantum Hall regime," Phys. Rev. B **86**, 081410 (2012).
[198]H. Hettmansperger, F. Duerr, J. B. Oostinga, C. Gould, B. Trauzettel, and L. W. Molenkamp, "Quantum Hall effect in narrow graphene ribbons," Phys. Rev. B **86**, 195417 (2012).
[199]Z. B. Tan, A. Puska, T. Nieminen, F. Duerr, C. Gould, L. W. Molenkamp, B. Trauzettel, and P. J. Hakonen, "Shot noise in lithographically patterned graphene nanoribbons," Phys. Rev. B **88**, 245415 (2013).
[200]F. Molitor, A. Jacobsen, C. Stampfer, J. Güttinger, T. Ihn, and K. Ensslin, "Transport gap in side-gated graphene constrictions," Phys. Rev. B **79**, 075426 (2009).
[201]C. Stampfer, J. Güttinger, S. Hellmüller, F. Molitor, K. Ensslin, and T. Ihn, "Energy gaps in etched graphene nanoribbons," Phys. Rev. Lett. **102**, 056403 (2009).
[202]F. Molitor, C. Stampfer, J. Güttinger, A. Jacobsen, T. Ihn, and K. Ensslin, "Energy and transport gaps in etched graphene nanoribbons," Semicond. Sci. Technol. **25**, 034002 (2010).
[203]S. Dröscher, H. Knowles, Y. Meir, K. Ensslin, and T. Ihn, "Coulomb gap in graphene nanoribbons," Phys. Rev. B **84**, 073405 (2011).
[204]B. Terrés, J. Dauber, C. Volk, S. Trellenkamp, U. Wichmann, and C. Stampfer, "Disorder induced Coulomb gaps in graphene constrictions with different aspect ratios," Appl. Phys. Lett. **98**, 032109 (2011).
[205]D. Bischoff, T. Krähenmann, S. Dröscher, M. A. Gruner, C. Barraud, T. Ihn, and K. Ensslin, "Reactive-ion-etched graphene nanoribbons on a hexagonal boron nitride substrate," Appl. Phys. Lett. **101**, 203103 (2012).
[206]N. Pascher, D. Bischoff, T. Ihn, and K. Ensslin, "Scanning gate microscopy on a graphene nanoribbon," Appl. Phys. Lett. **101**, 063101 (2012).
[207]S. Engels, P. Weber, B. Terres, J. Dauber, C. Meyer, C. Volk, S. Trellenkamp, U. Wichmann, and C. Stampfer, "Fabrication of coupled graphene–nanotube quantum devices," Nanotechnology **24**, 035204 (2013).
[208]E. U. Stutzel, T. Dufaux, A. Sagar, S. Rauschenbach, K. Balasubramanian, M. Burghard, and K. Kern, "Spatially resolved photocurrents in graphene nanoribbon devices," Appl. Phys. Lett. **102**, 043106 (2013).
[209]D. Bischoff, F. Libisch, J. Burgdörfer, T. Ihn, and K. Ensslin, "Characterizing wave functions in graphene nanodevices: Electronic transport through ultrashort graphene constrictions on a boron nitride substrate," Phys. Rev. B **90**, 115405 (2014).
[210]D. Bischoff, M. Eich, A. Varlet, P. Simonet, T. Ihn, and K. Ensslin, "Measuring the local quantum capacitance of graphene using a strongly coupled graphene nanoribbon," Phys. Rev. B **91**, 115441 (2015).
[211]C. W. Smith, J. Katoch, and M. Ishigami, "Impact of charge impurities on transport properties of graphene nanoribbons," Appl. Phys. Lett. **102**, 133502 (2013).

[212]X. Li, X. Wang, L. Zhang, S. Lee, and H. Dai, "Chemically derived, ultrasmooth graphene nanoribbon semiconductors," Science **319**, 1229–1232 (2008).
[213]X. Wang, Y. Ouyang, X. Li, H. Wang, J. Guo, and H. Dai, "Room-temperature all-semiconducting sub-10-nm graphene nanoribbon field-effect transistors," Phys. Rev. Lett. **100**, 206803 (2008).
[214]J.-M. Poumirol, A. Cresti, S. Roche, W. Escoffier, M. Goiran, X. Wang, X. Li, H. Dai, and B. Raquet, "Edge magnetotransport fingerprints in disordered graphene nanoribbons," Phys. Rev. B **82**, 041413 (2010).
[215]L. Jiao, L. Zhang, X. Wang, G. Diankov, and H. Dai, "Narrow graphene nanoribbons from carbon nanotubes," Nature **458**, 877–880 (2009).
[216]D. V. Kosynkin, A. L. Higginbotham, A. Sinitskii, J. R. Lomeda, A. Dimiev, B. K. Price, and J. M. Tour, "Longitudinal unzipping of carbon nanotubes to form graphene nanoribbons," Nature **458**, 872–877 (2009).
[217]D. V. Kosynkin, W. Lu, A. Sinitskii, G. Pera, Z. Sun, and J. M. Tour, "Highly conductive graphene nanoribbons by longitudinal splitting of carbon nanotubes using potassium vapor," ACS Nano **5**, 968–974 (2011).
[218]M.-W. Lin, C. Ling, L. A. Agapito, N. Kioussis, Y. Zhang, M. M.-C. Cheng, W. L. Wang, E. Kaxiras, and Z. Zhou, "Approaching the intrinsic band gap in suspended high-mobility graphene nanoribbons," Phys. Rev. B **84**, 125411 (2011).
[219]M.-W. Lin, C. Ling, Y. Zhang, H. J. Yoon, M. M.-C. Cheng, L. A. Agapito, N. Kioussis, N. Widjaja, and Z. Zhou, "Room-temperature high on/off ratio in suspended graphene nanoribbon field-effect transistors," Nanotechnology **22**, 265201 (2011).
[220]T. Shimizu, J. Haruyama, D. C. Marcano, D. V. Kosinkin, J. M. Tour, K. Hirose, and K. Suenaga, "Large intrinsic energy bandgaps in annealed nanotube-derived graphene nanoribbons," Nat. Nanotechnol. **6**, 45–50 (2011).
[221]D. Wei, L. Xie, K. K. Lee, Z. Hu, S. Tan, W. Chen, C. H. Sow, K. Chen, Y. Liu, and A. T. S. Wee, "Controllable unzipping for intramolecular junctions of graphene nanoribbons and single-walled carbon nanotubes," Nat. Commun. **4**, 1374 (2013).
[222]S. Blankenburg, J. Cai, P. Ruffieux, R. Jaafar, D. Passerone, X. Feng, K. Mullen, R. Fasel, and C. A. Pignedoli, "Intraribbon heterojunction formation in ultranarrow graphene nanoribbons," ACS Nano **6**, 2020–2025 (2012).
[223]P. Ruffieux, J. Cai, N. C. Plumb, L. Patthey, D. Prezzi, A. Ferretti, E. Molinari, X. Feng, K. Mullen, C. A. Pignedoli, and R. Fasel, "Electronic structure of atomically precise graphene nanoribbons," ACS Nano **6**, 6930–6935 (2012).
[224]M. Koch, F. Ample, C. Joachim, and L. Grill, "Voltage-dependent conductance of a single graphene nanoribbon," Nat. Nanotechnol. **7**, 713–717 (2012).
[225]H. Huang, D. Wei, J. Sun, S. L. Wong, Y. P. Feng, A. H. C. Neto, and A. T. S. Wee, "Spatially resolved electronic structures of atomically precise armchair graphene nanoribbons," Sci. Rep. **2**, 983 (2012).
[226]J. van der Lit, M. P. Boneschanscher, D. Vanmaekelbergh, M. Ijäs, A. Uppstu, M. Ervasti, A. Harju, P. Liljeroth, and I. Swart, "Suppression of electron–vibron coupling in graphene nanoribbons contacted via a single atom," Nat. Commun. **4**, 2023 (2013).
[227]X. Wang and H. Dai, "Etching and narrowing of graphene from the edges," Nat. Chem. **2**, 661–665 (2010).
[228]J. Baringhaus, M. Ruan, F. Edler, A. Tejeda, M. Sicot, A. Taleb-Ibrahimi, A.-P. Li, Z. Jiang, E. H. Conrad, C. Berger, C. Tegenkamp1, and W. A. de Heer, "Exceptional ballistic transport in epitaxial graphene nanoribbons," Nature **506**, 349–354 (2014).
[229]M. S. Nevius, F. Wang, C. Mathieu, N. Barrett, A. Sala, T. O. Mentes, A. Locatelli, and E. H. Conrad, "The bottom-up growth of edge specific graphene nano-ribbons," Nano Lett. **14**, 6080–6086 (2014).
[230]S. Masubuchi, M. Ono, K. Yoshida, K. Hirakawa, and T. Machida, "Fabrication of graphene nanoribbon by local anodic oxidation lithography using atomic force microscope," Appl. Phys. Lett. **94**, 082107 (2009).
[231]M. Moreno-Moreno, A. Castellanos-Gomez, G. Rubio-Bollinger, J. Gomez-Herrero, and N. Agrait, "Ultralong natural graphene nanoribbons and their electrical conductivity," Small **5**, 924–927 (2009).
[232]M. C. Lemme, D. C. Bell, J. R. Williams, L. A. Stern, B. W. H. Baugher, P. Jarillo-Herrero, and C. M. Marcus, "Etching of graphene devices with a helium ion beam," ACS Nano **3**, 2674–2676 (2009).
[233]A. N. Abbas, G. Liu, B. Liu, L. Zhang, H. Liu, D. Ohlberg, W. Wu, and C. Zhou, "Patterning, characterization, and chemical sensing applications of graphene nanoribbon arrays down to 5 nm using helium ion beam lithography," ACS Nano **8**, 1538–1546 (2014).
[234]A. M. Goossens, S. C. M. Driessen, T. A. Baart, K. Watanabe, T. Taniguchi, and L. M. K. Vandersypen, "Gate-defined confinement in bilayer graphene-hexagonal boron nitride hybrid devices," Nano Lett. **12**, 4656–4660 (2012).
[235]L. Tapaszto, G. Dobrik, P. Lambin, and L. P. Biro, "Tailoring the atomic structure of graphene nanoribbons by scanning tunneling microscope lithography," Nat. Nanotechnol. **3**, 397–401 (2008).
[236]L. C. Campos, V. R. Manfrinato, J. D. Sanchez-Yamagishi, J. Kong, and P. Jarillo-Herrero, "Anisotropic etching and nanoribbon formation in single-layer graphene," Nano Lett. **9**, 2600–2604 (2009).
[237]Y. Lu, B. Goldsmith, D. R. Strachan, J. H. Lim, Z. Luo, and A. T. C. Johnson, "High-on/off-ratio graphene nanoconstriction field-effect transistor," Small **6**, 2748–2754 (2010).
[238]T. Kato and R. Hatakeyama, "Site- and alignment-controlled growth of graphene nanoribbons from nickel nanobars," Nat. Nanotechnol. **7**, 651–656 (2012).
[239]C.-H. Huang, C.-Y. Su, T. Okada, L.-J. Li, K.-I. Ho, P.-W. Li, I.-H. Chen, C. Chou, C.-S. Lai, and S. Samukawa, "Ultra-low-edge-defect graphene nanoribbons patterned by neutral beam," Carbon **61**, 229–235 (2013).
[240]J. Moser and A. Bachtold, "Fabrication of large addition energy quantum dots in graphene," Appl. Phys. Lett. **95**, 173506 (2009).
[241]X.-X. Song, H.-O. Li, J. You, T.-Y. Han, G. Cao, T. Tu, M. Xiao, G.-C. Guo, H.-W. Jiang, and G.-P. Guo, "Suspending effect on low-frequency charge noise in graphene quantum dot," Sci. Rep. **5**, 8142 (2015).
[242]S. Engels, A. Epping, C. Volk, S. Korte, B. Voigtlander, K. Watanabe, T. Taniguchi, S. Trellenkamp, and C. Stampfer, "Etched graphene quantum dots on hexagonal boron nitride," Appl. Phys. Lett. **103**, 073113 (2013).
[243]A. Epping, S. Engels, C. Volk, K. Watanabe, T. Taniguchi, S. Trellenkamp, and C. Stampfer, "Etched graphene single electron transistors on hexagonal boron nitride in high magnetic fields," Phys. Status Solidi B **250**, 2692–2696 (2013).
[244]J. Güttinger, C. Stampfer, S. Hellmüller, F. Molitor, T. Ihn, and K. Ensslin, "Charge detection in graphene quantum dots," Appl. Phys. Lett. **93**, 212102 (2008).
[245]J. Güttinger, C. Stampfer, F. Molitor, D. Graf, T. Ihn, and K. Ensslin, "Coulomb oscillations in three-layer graphene nanostructures," New J. Phys. **10**, 125029 (2008).
[246]C. Stampfer, J. Güttinger, F. Molitor, D. Graf, T. Ihn, and K. Ensslin, "Tunable Coulomb blockade in nanostructured graphene," Appl. Phys. Lett. **92**, 012102 (2008).
[247]C. Stampfer, E. Schurtenberger, F. Molitor, J. Güttinger, T. Ihn, and K. Ensslin, "Tunable graphene single electron transistor," Nano Lett. **8**, 2378–2383 (2008).
[248]J. Güttinger, C. Stampfer, F. Libisch, T. Frey, J. Burgdörfer, T. Ihn, and K. Ensslin, "Electron-hole crossover in graphene quantum dots," Phys. Rev. Lett. **103**, 046810 (2009).
[249]J. Güttinger, C. Stampfer, T. Frey, T. Ihn, and K. Ensslin, "Graphene quantum dots in perpendicular magnetic fields," Phys. Status Solidi B **246**, 2553–2557 (2009).
[250]F. Molitor, S. Dröscher, J. Güttinger, A. Jacobsen, C. Stampfer, T. Ihn, and K. Ensslin, "Transport through graphene double dots," Appl. Phys. Lett. **94**, 222107 (2009).
[251]S. Schnez, F. Molitor, C. Stampfer, J. Güttinger, I. Shorubalko, T. Ihn, and K. Ensslin, "Observation of excited states in a graphene quantum dot," Appl. Phys. Lett. **94**, 012107 (2009).
[252]J. Güttinger, T. Frey, C. Stampfer, T. Ihn, and K. Ensslin, "Spin states in graphene quantum dots," Phys. Rev. Lett. **105**, 116801 (2010).
[253]X. L. Liu, D. Hug, and L. M. K. Vandersypen, "Gate-defined graphene double quantum dot and excited state spectroscopy," Nano Lett. **10**, 1623–1627 (2010).
[254]F. Molitor, H. Knowles, S. Dröscher, U. Gasser, T. Choi, P. Roulleau, J. Güttinger, A. Jacobsen, C. Stampfer, K. Ensslin, and T. Ihn, "Observation of excited states in a graphene double quantum dot," Europhys. Lett. **89**, 67005 (2010).
[255]P. Roulleau, S. Baer, T. Choi, F. Molitor, J. Güttinger, T. Müller, S. Dröscher, K. Ensslin, and T. Ihn, "Coherent electron–phonon coupling in tailored quantum systems," Nat. Commun. **2**, 239 (2011).
[256]S. Schnez, J. Güttinger, M. Huefner, C. Stampfer, K. Ensslin, and T. Ihn, "Imaging localized states in graphene nanostructures," Phys. Rev. B **82**, 165445 (2010).
[257]M. Arai, S. Masubuchi, and T. Machida, "Single-electron switching effect in graphene parallel-coupled double quantum dots," J. Phys.: Conf. Ser. **334**, 012041 (2011).

[258]S. Fringes, C. Volk, C. Norda, B. Terres, J. Dauber, S. Engels, S. Trellenkamp, and C. Stampfer, "Charge detection in a bilayer graphene quantum dot," Phys. Status Solidi B **248**, 2684–2687 (2011).
[259]J. Güttinger, J. Seif, C. Stampfer, A. Capelli, K. Ensslin, and T. Ihn, "Time-resolved charge detection in graphene quantum dots," Phys. Rev. B **83**, 165445 (2011).
[260]J. Güttinger, C. Stampfer, T. Frey, T. Ihn, and K. Ensslin, "Transport through a strongly coupled graphene quantum dot in perpendicular magnetic field," Nanoscale Res. Lett. **6**, 253 (2011).
[261]C. Volk, S. Fringes, B. Terrees, J. Dauber, S. Engels, S. Trellenkamp, and C. Stampfer, "Electronic excited states in bilayer graphene double quantum dots," Nano Lett. **11**, 3581–3586 (2011).
[262]L.-J. Wang, G.-P. Guo, D. Wei, G. Cao, T. Tu, M. Xiao, G.-C. Guo, and A. M. Chang, "Gates controlled parallel-coupled double quantum dot on both single layer and bilayer graphene," Appl. Phys. Lett. **99**, 112117 (2011).
[263]S. Dröscher, J. Güttinger, T. Mathis, B. Batlogg, T. Ihn, and K. Ensslin, "High-frequency gate manipulation of a bilayer graphene quantum dot," Appl. Phys. Lett. **101**, 043107 (2012).
[264]S. Fringes, C. Volk, B. Terres, J. Dauber, S. Engels, S. Trellenkamp, and C. Stampfer, "Tunable capacitive inter-dot coupling in a bilayer graphene double quantum dot," Phys. Status Solidi C **9**, 169–174 (2012).
[265]A. Jacobsen, P. Simonet, K. Ensslin, and T. Ihn, "Transport in a three-terminal graphene quantum dot in the multi-level regime," New J. Phys. **14**, 023052 (2012).
[266]T. Müller, J. Güttinger, D. Bischoff, S. Hellmüller, K. Ensslin, and T. Ihn, "Fast detection of single-charge tunneling to a graphene quantum dot in a multi-level regime," Appl. Phys. Lett. **101**, 012104 (2012).
[267]C. Neumann, C. Volk, S. Engels, and C. Stampfer, "Graphene-based charge sensors," Nanotechnology **24**, 444001 (2013).
[268]C. Volk, C. Neumann, S. Kazarski, S. Fringes, S. Engels, F. Haupt, A. Müller, and C. Stampfer, "Probing relaxation times in graphene quantum dots," Nat. Commun. **4**, 1753 (2013).
[269]S. Moriyama, D. Tsuya, E. Watanabe, S. Uji, M. Shimizu, T. Mori, T. Yamaguchi, and K. Ishibashi, "Coupled quantum dots in a graphene-based two-dimensional semimetal," Nano Lett. **9**, 2891–2896 (2009).
[270]S. Moriyama, Y. Morita, E. Watanabe, D. Tsuya, S. Uji, M. Shimizu, and K. Ishibashi, "Fabrication of quantum-dot devices in graphene," Sci. Technol. Adv. Mater. **11**, 054601 (2010).
[271]L.-J. Wang, G. Cao, T. Tu, H.-O. Li, C. Zhou, X.-J. Hao, Z. Su, G.-C. Guo, H.-W. Jiang, and G.-P. Guo, "A graphene quantum dot with a single electron transistor as an integrated charge sensor," Appl. Phys. Lett. **97**, 262113 (2010).
[272]L.-J. Wang, H.-O. Li, T. Tu, G. Cao, C. Zhou, X.-J. Hao, Z. Su, M. Xiao, G.-C. Guo, A. M. Chang, and G.-P. Guo, "Controllable tunnel coupling and molecular states in a graphene double quantum dot," Appl. Phys. Lett. **100**, 022106 (2012).
[273]M. R. Connolly, K. L. Chiu, S. P. Giblin, M. Kataoka, J. D. Fletcher, C. Chua, J. P. Griffiths, G. A. C. Jones, V. I. Fal'ko, C. G. Smith, and T. J. B. M. Janssen, "Gigahertz quantized charge pumping in graphene quantum dots," Nat. Nanotechnol. **8**, 417–420 (2013).
[274]A. Müller, B. Kaestner, F. Hohls, T. Weimann, K. Pierz, and H. W. Schumacher, "Bilayer graphene quantum dot defined by topgates," J. Appl. Phys. **115**, 233710 (2014).
[275]A. Barreiro, H. S. J. van der Zant, and L. M. K. Vandersypen, "Quantum dots at room temperature carved out from few-layer graphene," Nano Lett. **12**, 6096–6100 (2012).
[276]S. Neubeck, L. A. Ponomarenko, F. Freitag, A. J. M. Giesbers, U. Zeitler, S. V. Morozov, P. Blake, A. K. Geim, and K. S. Novoselov, "From one electron to one hole: Quasiparticle counting in graphene quantum dots determined by electrochemical and plasma etching," Small **6**, 1469–1473 (2010).
[277]R. K. Puddy, C. J. Chua, and M. R. Buitelaar, "Transport spectroscopy of a graphene quantum dot fabricated by atomic force microscope nanolithography," Appl. Phys. Lett. **103**, 183117 (2013).
[278]L. A. Ponomarenko, F. Schedin, M. I. Katsnelson, R. Yang, E. W. Hill, K. S. Novoselov, and A. K. Geim, "Chaotic Dirac billiard in graphene quantum dots," Science **320**, 356–358 (2008).
[279]J. S. Bunch, Y. Yaish, M. Brink, K. Bolotin, and P. L. McEuen, "Coulomb oscillations and Hall effect in quasi-2D graphite quantum dots," Nano Lett. **5**, 287–290 (2005).
[280]T. Ihn, *Semiconductor Nanostructures: Quantum States and Electronic Transport* (Oxford University Press, 2009).
[281]C. W. J. Beenakker and H. van Houten, "Quantum transport in semiconductor nanostructures," Solid State Phys. **44**, 1–228 (1991).
[282]L. P. Kouwenhoven, T. H. Oosterkamp, M. W. S. Danoesastro, M. Eto, D. G. Austing, T. Honda, and S. Tarucha, "Excitation spectra of circular, few-electron quantum dots," Science **278**, 1788–1792 (1997).
[283]L. P. Kouwenhoven, D. G. Austing, and S. Tarucha, "Few-electron quantum dots," Rep. Prog. Phys. **64**, 701–736 (2001).
[284]H. van Houten, C. W. J. Beenakker, and A. A. M. Staring, "Coulomb-blockade oscillations in semiconductor nanostructures," *Single Charge Tunneling and Coulomb Blockade Phenomena in Nanostructures* (Springer, 1992).
[285]W. G. van der Wiel, S. De Franceschi, J. M. Elzerman, T. Fujisawa, S. Tarucha, and L. P. Kouwenhoven, "Electron transport through double quantum dots," Rev. Mod. Phys. **75**, 1–22 (2002).
[286]While a band gap is a "bulk" material property, a confinement gap could arise due to the finite size of the device in analogy to a "particle in a box."
[287]D. A. Wharam, T. J. Thornton, R. Newbury, M. Pepper, H. Ahmed, J. E. F. Frost, D. G. Hasko, D. C. Peacock, D. A. Ritchie, and G. A. C. Jones, "One-dimensional transport and the quantisation of the ballistic resistance," J. Phys. C: Solid State Phys. **21**, L209 (1988).
[288]B. J. van Wees, H. van Houten, C. W. J. Beenakker, J. G. Williamson, L. P. Kouwenhoven, D. van der Marel, and C. T. Foxon, "Quantized conductance of point contacts in a two-dimensional electron gas," Phys. Rev. Lett. **60**, 848–850 (1988).
[289]J. Nygard, D. H. Cobden, and P. E. Lindelof, "Kondo physics in carbon nanotubes," Nature **408**, 342–346 (2000).
[290]H. O. H. Churchill, A. J. Bestwick, J. W. Harlow, F. Kuemmeth, D. Marcos, C. H. Stwertka, S. K. Watson, and C. M. Marcus, "Electron–nuclear interaction in 13C nanotube double quantum dots," Nat. Phys. **5**, 321–326 (2009).
[291]M. R. Buitelaar, J. Fransson, A. L. Cantone, C. G. Smith, D. Anderson, G. A. C. Jones, A. Ardavan, A. N. Khlobystov, A. A. R. Watt, K. Porfyrakis, and G. A. D. Briggs, "Pauli spin blockade in carbon nanotube double quantum dots," Phys. Rev. B **77**, 245439 (2008).
[292]P. Fallahi, A. C. Bleszynski, R. M. Westervelt, J. Huang, J. D. Walls, E. J. Heller, M. Hanson, and A. C. Gossard, "Imaging a single-electron quantum dot," Nano Lett. **5**, 223–226 (2005).
[293]W. Liang, M. Bockrath, and H. Park, "Shell filling and exchange coupling in metallic single-walled carbon nanotubes," Phys. Rev. Lett. **88**, 126801 (2002).
[294]D. H. Cobden and J. Nygard, "Shell filling in closed single-wall carbon nanotube quantum dots," Phys. Rev. Lett. **89**, 046803 (2002).
[295]E. B. Foxman, U. Meirav, P. L. McEuen, M. A. Kastner, O. Klein, P. A. Belk, D. M. Abusch, and S. J. Wind, "Crossover from single-level to multilevel transport in artificial atoms," Phys. Rev. B **50**, 14193–14199 (1994).
[296]M. Pierre, M. Hofheinz, X. Jehl, M. Sanquer, G. Molas, M. Vinet, and S. Deleonibus, "Background charges and quantum effects in quantum dots transport spectroscopy," Eur. Phys. J. B **70**, 475–481 (2009).
[297]R. Leturcq, C. Stampfer, K. Inderbitzin, L. Durrer, C. Hierold, E. Mariani, M. G. Schultz, F. v. Oppen, and K. Ensslin, "Franck-condon blockade in suspended carbon nanotube quantum dots," Nat. Phys. **5**, 327–331 (2009).
[298]T. Schmidt, R. J. Haug, K. v. Klitzing, A. Förster, and H. Lüth, "Spectroscopy of the single-particle states of a quantum-dot molecule," Phys. Rev. Lett. **78**, 1544–1547 (1997).
[299]W. H. Lim, F. A. Zwanenburg, H. Huebl, M. Möttönen, K. W. Chan, A. Morello, and A. S. Dzurak, "Observation of the single-electron regime in a highly tunable silicon quantum dot," Appl. Phys. Lett. **95**, 242102 (2009).
[300]S. K. Hämäläinen, Z. Sun, M. P. Boneschanscher, A. Uppstu, M. Ijäs, A. Harju, D. Vanmaekelbergh, and P. Liljeroth, "Quantum-confined electronic states in atomically well-defined graphene nanostructures," Phys. Rev. Lett. **107**, 236803 (2011).
[301]S.-H. Phark, J. Borme, A. L. Vanegas, M. Corbetta, D. Sander, and J. Kirschner, "Direct observation of electron confinement in epitaxial graphene nanoislands," ACS Nano **5**, 8162–8166 (2011).
[302]D. Subramaniam, F. Libisch, Y. Li, C. Pauly, V. Geringer, R. Reiter, T. Mashoff, M. Liebmann, J. Burgdorfer, C. Busse, T. Michely, R. Mazzarello, M. Pratzer, and M. Morgenstern, "Wave-function mapping of graphene quantum dots with soft confinement," Phys. Rev. Lett. **108**, 046801 (2012).
[303]F. Craes, S. Runte, J. Klinkhammer, M. Kralj, T. Michely, and C. Busse, "Mapping image potential states on graphene quantum dots," Phys. Rev. Lett. **111**, 056804 (2013).
[304]W. Jolie, F. Craes, M. Petrovic, N. Atodiresei, V. Caciuc, S. Blügel, M. Kralj, T. Michely, and C. Busse, "Confinement of Dirac electrons in graphene quantum dots," Phys. Rev. B **89**, 155435 (2014).

[305]M. Bacon, S. J. Bradley, and T. Nann, "Graphene quantum dots," Part. Part. Syst. Charact. **31**, 415–428 (2014).
[306]R. Ye, C. Xiang, J. Lin, Z. Peng, K. Huang, Z. Yan, N. P. Cook, E. L. G. Samuel, C.-C. Hwang, G. Ruan, G. Ceriotti, A.-R. O. Raji, A. A. Marti, and J. M. Tour, "Coal as an abundant source of graphene quantum dots," Nat. Commun. **4**, 2943 (2013).
[307]X. Yan, X. Cui, B. Li, and L. Li, "Large, solution-processable graphene quantum dots as light absorbers for photovoltaics," Nano Lett. **10**, 1869–1873 (2010).
[308]K. J. Williams, C. A. Nelson, X. Yan, L.-S. Li, and X. Zhu, "Hot electron injection from graphene quantum dots to TiO_2," ACS Nano **7**, 1388–1394 (2013).
[309]Y. Li, Y. Zhao, H. Cheng, Y. Hu, G. Shi, L. Dai, and L. Qu, "Nitrogen-doped graphene quantum dots with oxygen-rich functional groups," J. Am. Chem. Soc. **134**, 15–18 (2012).
[310]L. Tang, R. Ji, X. Cao, J. Lin, H. Jiang, X. Li, K. S. Teng, C. M. Luk, S. Zeng, J. Hao, and S. P. Lau, "Deep ultraviolet photoluminescence of water-soluble self-passivated graphene quantum dots," ACS Nano **6**, 5102–5110 (2012).
[311]Z. Liu, L. Ma, G. Shi, W. Zhou, Y. Gong, S. Lei, X. Yang, J. Zhang, J. Yu, K. P. Hackenberg, A. Babakhani, J.-C. Idrobo, R. Vajtai, J. Lou, and P. M. Ajayan, "In-plane heterostructures of graphene and hexagonal boron nitride with controlled domain sizes," Nat. Nanotechnol. **8**, 119–124 (2013).
[312]Q. Xu, Q. Zhou, Z. Hua, Q. Xue, C. Zhang, X. Wang, D. Pan, and M. Xiao, "Single-particle spectroscopic measurements of fluorescent graphene quantum dots," ACS Nano **7**, 10654–10661 (2013).
[313]J. Peng, W. Gao, B. K. Gupta, Z. Liu, R. Romero-Aburto, L. Ge, L. Song, L. B. Alemany, X. Zhan, G. Gao, S. A. Vithayathil, B. A. Kaipparettu, A. A. Marti, T. Hayashi, J.-J. Zhu, and P. M. Ajayan, "Graphene quantum dots derived from carbon fibers," Nano Lett. **12**, 844–849 (2012).
[314]D. Pan, J. Zhang, Z. Li, and M. Wu, "Hydrothermal route for cutting graphene sheets into blue-luminescent graphene quantum dots," Adv. Mater. **22**, 734–738 (2010).
[315]H. Sun, L. Wu, W. Wei, and X. Qu, "Recent advances in graphene quantum dots for sensing," Mater. Today **16**, 433–442 (2013).
[316]M. L. Mueller, X. Yan, J. A. McGuire, and L. Li, "Triplet states and electronic relaxation in photoexcited graphene quantum dots," Nano Lett. **10**, 2679–2682 (2010).
[317]D. Joung, L. Zhai, and S. I. Khondaker, "Coulomb blockade and hopping conduction in graphene quantum dots array," Phys. Rev. B **83**, 115323 (2011).
[318]N. N. Klimov, S. Jung, S. Zhu, T. Li, C. A. Wright, S. D. Solares, D. B. Newell, N. B. Zhitenev, and J. A. Stroscio, "Electromechanical properties of graphene drumheads," Science **336**, 1557–1561 (2012).
[319]M. Chhowalla, H. S. Shin, G. Eda, L.-J. Li, K. P. Loh, and H. Zhang, "The chemistry of two-dimensional layered transition metal dichalcogenide nanosheets," Nat. Chem. **5**, 263–275 (2013).
[320]K. S. Novoselov, A. K. Geim, S. V. Morozov, D. Jiang, M. I. Katsnelson, I. V. Grigorieva, S. V. Dubonos, and A. A. Firsov, "Two-dimensional gas of massless Dirac fermions in graphene," Nature **438**, 197–200 (2005).
[321]L. Li, Y. Yu, G. J. Ye, Q. Ge, X. Ou, H. Wu, D. Feng, X. H. Chen, and Y. Zhang, "Black phosphorus field-effect transistors," Nat. Nanotechnol. **9**, 372–377 (2014).
[322]C. N. R. Rao, H. S. S. R. Matte, and U. Maitra, "Graphene analogues of inorganic layered materials," Angew. Chem. **52**, 13162–13185 (2013).
[323]V. Nicolosi, M. Chhowalla, M. G. Kanatzidis, M. S. Strano, and J. N. Coleman, "Liquid exfoliation of layered materials," Science **340**, 1226419 (2013).
[324]C. Kittel, *Einführung in die Festkörperphysik* (Oldenbourg Verlag München Wien, 2006), Vol. 14, pp. 181–206.
[325]R. S. Sundaram, M. Engel, A. Lombardo, R. Krupke, A. C. Ferrari, Ph. Avouris, and M. Steiner, "Electroluminescence in single layer MoS_2," Nano Lett. **13**, 1416–1421 (2013).
[326]A. Damascelli, "Probing the electronic structure of complex systems by ARPES," Phys. Scr. **2004**, 61–74 (2004).
[327]R. M. Feenstra, V. Ramachandran, and H. Chen, "Recent developments in scanning tunneling spectroscopy of semiconductor surfaces," Appl. Phys. A **72**, S193–S199 (2001).
[328]N. W. Ashcroft and N. D. Mermin, *Solid State Physics* (Brooks/Cole, 1976).
[329]H. Ibach and H. Lüth, *Festkörperphysik* (Springer, 2009), Vol. 7.